Journal of Medicinal Chemistry

Article

Discovery of Non-Quinone Substrates for NAD(P)H: Quinone Oxidoreductase 1 (NQO1) as Effective Intracellular ROS Generators for the Treatment of Drug-Resistant Non-Small Cell Lung Cancer

Xingsen Wu, Xiang Li, Zhihong Li, Yancheng Yu, Qi-Dong You, and Xiaojin Zhang

J. Med. Chem., **Just Accepted Manuscript** • DOI: 10.1021/acs.jmedchem.8b01424 • Publication Date (Web): 03 Dec 2018

Discovery of Non-Quinone Substrates for NAD(P)H: Quinone Oxidoreductase 1 (NQO1) as Effective Intracellular ROS Generators for the Treatment of Drug-Resistant Non-Small Cell Lung Cancer

Xingsen Wu, [†,‡] *Xiang Li,* [†,§] *Zhihong Li,* [†,‡] *Yancheng Yu,* [†,‡] *Qidong You,* [*,†] *Xiaojin Zhang* [*,†,‡]

[†] State Key Laboratory of Natural Medicines and Jiangsu Key Laboratory of Drug Design and Optimization, China Pharmaceutical University, Nanjing, 210009, China

[‡] Department of Chemistry, School of Science, China Pharmaceutical University, Nanjing, 21119, China

[§] Department of Pharmaceutical Engineering, China Pharmaceutical University, Nanjing, 21119, China

[*] Corresponding authors. E-mail: youqd@163.com (Q. You), zxj@cpu.edu.cn (X. Zhang)

ABSTRACT.

The elevation of oxidative stress preferentially in cancer cells by efficient NQO1 substrates which promote ROS generation through redox cycling has emerged as an effective strategy for cancer therapy, even for treating drug-resistant cancers. Here, we described the identification and structural optimization studies of the hit compound **1**, a new chemotype of non-quinone substrate for NQO1 as an efficient ROS generator. Further structure-activity relationship studies resulted in the most active compound **20k**, a tricyclic 2,3-dicyano indenopyrazinone, which selectively inhibited the proliferation of NQO1-overexpressing A549 and A549/Taxol cancer cells. Furthermore, **20k** dramatically elevated the intracellular ROS levels through NQO1-catalyzed redox cycling, and induced PARP-1-mediated cell apoptosis in A549/Taxol cells. In addition, **20k** significantly suppressed the growth of A549/Taxol xenograft tumors in mice with no apparent toxicity observed in vivo. Together, **20k** acts as an efficient NQO1 substrate and may be a new option for the treatment of NQO1-overexpresssing drug-resistant NSCLC.

KEYWORDS

NQO1, Non-quinone substrates, ROS, Drug-resistant, NSCLC

1. INTRODUCTION

Non-small cell lung cancer (NSCLC) is one of the common aggressive malignant tumor accounting for approximately 85% of human lung cancer, a disease which remains the leading cause of cancer-related mortality worldwide.[1] The overall 5-year survival rate for NSCLC (all stages combined) is roughly 17% and the 5-year survival rate in stage IV is only about 2%.[2] Although the treatment of NSCLC has evolved over the past two decades resulting in different therapeutic options including chemotherapy,[3] tyrosine kinase inhibitors,[4] monoclonal antibodies,[5,6] and some combinations,[7] great challenges still exist due to the intrinsic or acquired drug resistance and genomic instability in cancers.[8] For instance, taxol, a chemotherapy drug for the first-line treatment of NSCLC, almost universally fail for late-stage NSCLC patients owing to drug resistance.[9] Therefore, new drugs and new strategies for effective treatment of drug resistant NSCLC are urgent needs to develop.

Modulation of the unique biochemical alterations in cancer cells provides a new approach for cancer therapy, and probably prevents the development of drug resistance.[10] Reactive oxygen species (ROS) at low levels play important roles as second messengers in several cellular processes such as proliferation, angiogenesis, and metastasis.[11,12] However, when present at high levels, ROS irreversibly damage DNA, lipids, and proteins, and ultimately cause apoptosis of cancer cells.[13] It is worth noting that cancer cells are usually exposed to a relatively high level of ROS compared to that for normal cells.[14] Such biochemical differences make cancer cells more susceptible to induced oxidative stress, exceed the threshold that they can endure and lead to ROS-mediated cell death.[15-17] Therefore, pharmacological elevation of intracellular ROS level by small molecules has been regarded as an effective strategy for cancer therapy.[18-20] Moreover, the efficacy of this ROS-generating method has been demonstrated in some drug-resistance cancers.[21] Cotreatment of the

molecules that mediate their effects through a ROS based mechanism with anticancer drugs has significantly sensitized the cells to drugs by overcoming the resistance.[22,23] Thus, the strategy to develop ROS-generating molecules could be promising in treating drug-resistance cancers.

A crucial issue in developing ROS-generating strategy is how to elevate the levels of ROS specifically in cancer cells while simultaneously sparing normal cells. In this respect, NAD(P)H: quinone oxidoreductase (NQO1) and its redox substrates are being paid close attention to gradually.[24-26] NQO1 is such a cancer-specific cytosolic flavoenzyme that is highly elevated in multiple cancer cells, especially in NSCLC cells,[27] where it is constitutively overexpressed over 100-fold greater than that in correlative normal tissues.[28] NQO1 uses the reduced pyridine nucleotide NADH or NADPH as cofactor to catalyze the direct two-electron reduction of a wide variety of quinones to give hydroquinones (Figure 1A).[29,30] Many efficient NQO1 substrates have been reported to be potential antitumor drugs and the three main mechanisms are described as follows: 1) a direct alkylation of DNA by the corresponding hydroquinones formed by NQO1 bioreduction (e.g., mitomycin C); 2) hydroquinones as potent Hsp90 inhibitors (e.g., geldamycin and its derivative 17-AAG); 3) rapid generation of ROS through redox cycling between hydroquinones and its quinone substrates, such as β-lapachone (β-lap, Figure 1B) (an antitumor drug candidate in multiple clinical trials),[31] deoxynyboquinone (DNQ, Figure 1B),[32] streptonigrin (STN),[33] and their derivatives.[34] The last mode-of-action by redox cycling is the most substantiated NQO1-dependent mechanism for anticancer quinones. Upon bioreductive activation of certain quinones, the corresponding unstable hydroquinones rapidly react with physiological oxygen (O_2) in cells to provide two equivalent of superoxide ($O_2^{\bullet-}$), the main constitute of ROS, and regenerate the quinones (Figure 1A).[35] Due to the fact that these redox substrates rapidly and catalytically generate a great amount of toxic ROS specifically in NQO1-overexpressing cells, they have

considerable potential as efficient ROS generators for cancer treatment. However, what cannot be ignored is that all the present NQO1-mediated ROS generators via redox cycling, structurally, contain a quinone moiety (Figure 1B), which is often considered as a structural alert as applied in medicinal chemistry for the risk of idiosyncratic drug toxicity, owing to its reactivity toward cellular nucleophiles through Michael addition.[36,37]

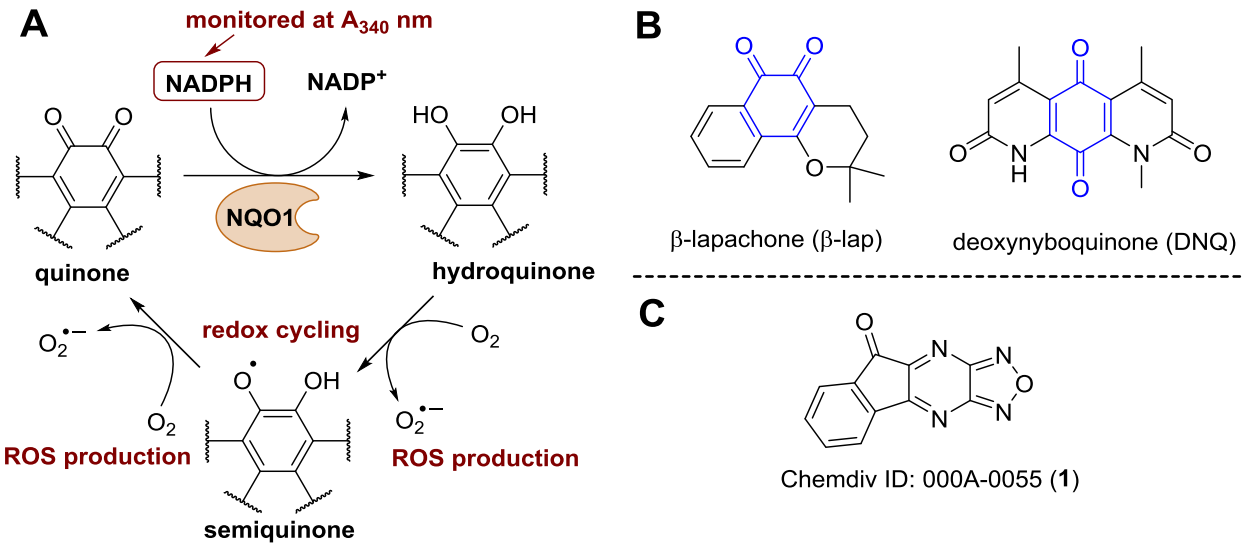

Figure 1. (A) Redox cycling of quinone substrates for NQO1, and the principle of NADPH-based NQO1 assay for screening new redox cycling NQO1 substrates; (B) Representative NQO1-mediated redox cycling quinones as antitumor ROS generators; (C) Structure of hit compound **1** as non-quinone redox cycling substrate for NQO1 in this work.

Here, we report our efforts on the discovery of non-quinone substrates for NQO1 as effective intracellular ROS generators for the treatment of drug-resistant NSCLC. Through screening of an in-house collection of 7500 compounds by using an NADPH-based NQO1 assay, fortunately, compound **1** was identified as an efficient ROS generator through NQO1-catalyzed redox cycling with a tetracyclic non-quinone scaffold. It exerted significant antitumor activities in

vitro toward both A549 and taxol-resistant A549/Taxol lung cancer cells, and showed considerable selectivity to NQO1-rich A549/Taxol cancer cells over NQO1-deficient L02 normal hepatic cells. Thus, tetracyclic compound **1** was selected as a starting point for optimization. Then, compound **20k** with a simplified tricyclic scaffold, which was more selective toward A549/Taxol cancer cells, was revealed from the structure-activity relationship (SAR) study by a step-by-step modification strategy. Pharmacological study demonstrated that **20k** dramatically elevated the intracellular ROS levels through NQO1-catalyzed redox cycling, and induced poly(ADP-ribose)polymerase-1 (PARP-1)-mediated cell apoptosis in an NQO1- and ROS-dependent manner in A549/Taxol cells. It also significally suppressed tumor growth in A549/Taxol cell-xenografted mouse model with no apparent toxicity observed in vivo. Therefore, we provide a new chemotype of non-quinone substrates for NQO1 as effective and selective intracellular ROS generators for developing promising new drugs for the treatment of NQO1-overexpresssing drug-resistant NSCLC.

2. RESULTS AND DISCUSSION

2.1. Hit Identification from an In-House Compound Collection Using an NADPH-Based NQO1 Assay. *Screening for Non-quinone Redox Cycling NQO1 Substrates as ROS Generators.* With the aim to discover new chemical types of NQO1 substrates with redox cycling property, we screened experimentally an in-house compound collection containing 7500 compounds by using an NADPH-based NQO1 assay.[38] As illustrated in Figure 1A, given that the tested compound acted as an NQO1 substrate and formed redox cycling, the amount of consumed NADPH would be much more than that of tested compound. N (cycles), defined as the equiv of consumed NADPH divided by the equiv of tested compound, was used as an index to the character of redox cycling. Compounds with N (cycles) > 10 (half of the N value of positive control quinone substrate β-lap) were selected as hit compounds. Fortunately, non-quinone compound **1** (Chemdiv

ID: 000A-0055, Figure 1C), was revealed as an efficient redox cycling NQO1 substrate with an N (cycles) value of 23, which was comparable to that of well-known quinone substrate β-lap (Figure 2A). Moreover, when compound **1** was tested in the absence of NQO1 or with the addition of an NQO1 inhibitor dicoumarol (DIC), no or little amount of NAPDH was consumed, indicating that the redox cycling of **1** relied on NQO1 bioreduction (Figure 2A). Further, by quantifying NADPH oxidation at 2 s intervals in the initial 5 min under different concentrations of **1**, the NQO1 reduction rates (Figure 2B) and Michaelis-Menten curves (Figure 2C) were generated, and the apparent catalytic efficiencies were calculated. It was observed that compound **1** was a highly efficient substrate and redox cycler with a reduction rate of 1412 ± 64 μmol NADPH/min/μmol NQO1 at 10 μM, and a k_{cat}/K_M value of 5.8 ± 1.0 × 10^6 $M^{-1}s^{-1}$, which was processed much faster than β-lap (reduction rate = 1155 ± 44 μmol NADPH/min/μmol NQO1 at 10 μM, and k_{cat}/K_M = 4.4 ± 0.9 × 10^6 $M^{-1}s^{-1}$). Considering that the redox cycling could lead to ROS generation, we thus set out to identify the ability of **1** to generate ROS. The generation of superoxide ($O_2^{\bullet-}$) was measured by a spectrophotometric assay using cytochrome *c* as the terminal electron acceptor.[39] As shown in Figure 2D, non-quinone compound **1** showed rapid rate of ROS generation (ROS generation rate = 1092 ± 64 μmol cyt c/min/mg NQO1), being much more efficient than β-lap (ROS generation rate = 724 ± 7 μmol cyt c/min/mg NQO1). Additionally. coincubation with DIC dramatically reduced the rate of ROS generation by **1** (Figure 2D). These results indicated that the hit compound **1** could generate a high level of ROS via NQO1-directed redox cycling.

*Hit Compound **1** Exhibited Potent and Selective Cytotoxicity toward NQO1-Overespressing Drug Resistant NSCLC cells In Vitro*. Cytotoxicity studies were performed on hit compound **1** with cell survival being determined by the 3-(4, 5-dimethylthiazol-2-yl)-2,5-diphenyltetrazolium bromide (MTT) colorimetric assay against the human NSCLC cells, A549

(NQO1-rich) and drug-resistant A549/Taxol (NQO1-rich), and L02 normal hepatic cells (NQO1-deficient) (Figure S1). β-Lap was used as a positive control. Compound **1** showed potent cytotoxicity against NQO1-overexpressing A549 and A549/Taxol cells with IC_{50} values of 1.0 ± 0.2 μM (Figure 2E) and 0.6 ± 0.1 μM (Figure 2F), respectively, which was more active than β-lap. Whereas in the case of L02 cells, compound **1** was less sensitive with an IC_{50} of 14.3 ± 1.6 μM (Figure 2G). Of particular note was that non-quinone compound **1** showed considerable selectivity to drug-resistant NQO1-rich A549/Taxol cancer cells over NQO1-deficient L02 normal hepatic cells with a high selectivity ratio of 23.8, being much more selective than quinone compound β-lap (Figure H). Thus, compound **1** could be a promising hit for further optimization.

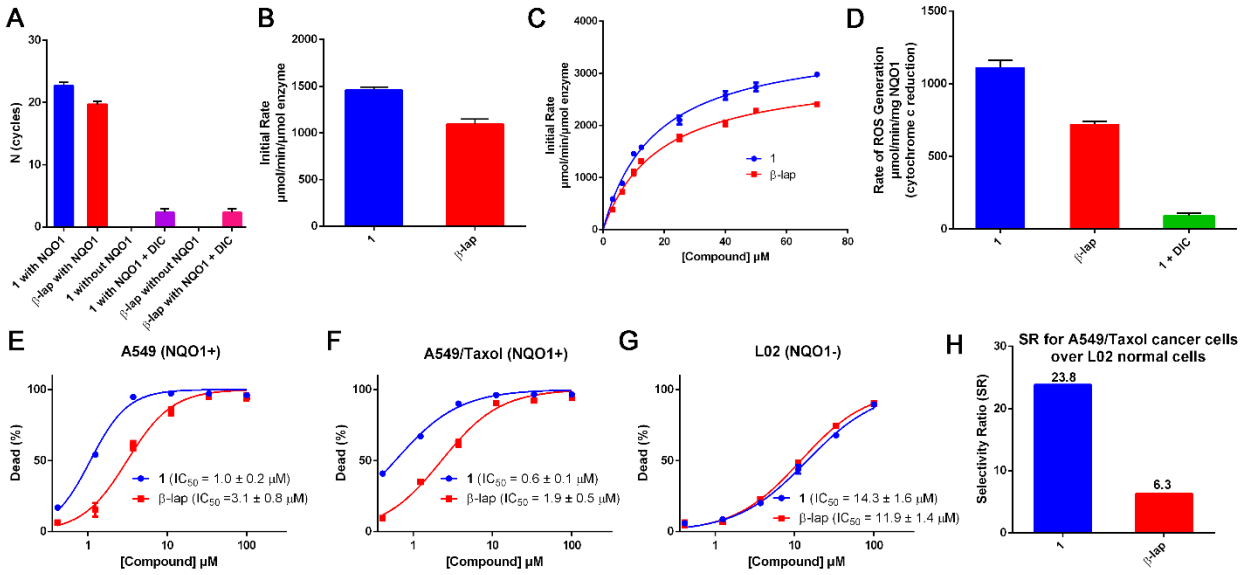

Figure 2. (A) N (cycles) represents that the equiv of NADPH consumed relatives to the equiv of substrates (10 μM) over the course of the NADPH-based NQO1 assay (in 5 min) monitored at 340 nm. (B) The initial reduction rates of non-quinone compound **1** and β-lap (10 μM) by NQO1. (C) Michaelis-Menten curves for **1** and β-lap with NQO1. (D) Rate of ROS production of **1** and β-lap in the presence and absence of the NQO1 inhibitor (DIC, 25 μM) with NQO1. (E) Cell death of NQO1-rich A549 cancer cells with **1** and β-lap for 72 h by MTT assay. (F) Cell death of NQO1-

rich A549/Taxol drug-resistant cancer cells with **1** and β-lap for 72 h by MTT assay. (G) Cell death of NQO1-deficient L02 normal hepatic cells with **1** and β-lap for 72 h by MTT assay. (H) The selectivity ratio (SR) toward NQO1-rich A549/Taxol cancer cells over NQO1-deficient L02 normal hepatic cells; SR = IC_{50} (L02)/IC_{50} (A549/Taxol).

2.2. SAR and Structural Modification of Compound 1 Utilizing a Step-By-Step Strategy. *SAR Studies Focusing on Rings C and D of Tetracyclic Compound **1** Resulting in Tricyclic Compound **10**.* To further optimization of hit compound **1**, a detailed SAR study was performed based on their NQO1 reduction rates in vitro. The target compounds **2-10** focusing on Rings D and C of **1** were designed as illustrated in Figure 3. Their reduction rates and N (cycles) by NQO1 were determined at the concentration of 10 μM by using the aforementioned NADPH-based assay, and the results were shown in Table 1. First, the oxadiazole ring D was converted into other aromatic rings such as benzene (**2-4**) and thiophene (**5**) as well as aliphatic ring such as cyclohexane (**6**), however, their NQO1 activities were dramatically decreased as compared to **1** with reduction rates ranging from 254 to 362 μmol NADPH/min/μmol NQO1. Removal of ring D as in compound **7** was also detrimental for its reduction activity by NQO1 (356 ± 41μmol NADPH/min/μmol NQO1). These results suggested that ring D of **1** was of great importance for its NQO1 reduction activity. Then, the pyrazine ring C of **7** was converted to 1,2,4-trazine as in compound **8**; no increased activity was observed. Moreover, the replacement of pyrazine ring C with benzene ring as in compound **9** led to a complete loss in activity, indicating that the nitrogen atoms in C ring were responsible for NQO1 reduction. Further, considering that the oxadiazole aromatic ring D of **1** probably acted as a delocalization moiety in the process of NQO1 reduction, we designed compound **10** with two cyano substitution directly linked to ring C by a ring opening strategy (Figure 3). The *sp* hybridized atoms in cyano group were expected to act similar function

to the oxadiazole ring D for electron delocalization during NQO1 reduction. Encouragingly, compound **10** exerted considerable activity to **1** as expected, with a reduction rate of 1362 ± 38 μmol NADPH/min/μmol NQO1, which was slightly more active than β-lap (1155 ± 44 μmol NADPH/min/μmol NQO1). Compound **10** was also an efficient redox cycler, showing twenty redox cycles in the presence of NQO1 in 5 min. It must be emphasized that compound **10** with a simplified indenopyrazinone tricylic scaffold, structurally, was more beneficial for further optimization than the tetracylic hit compound **1**.

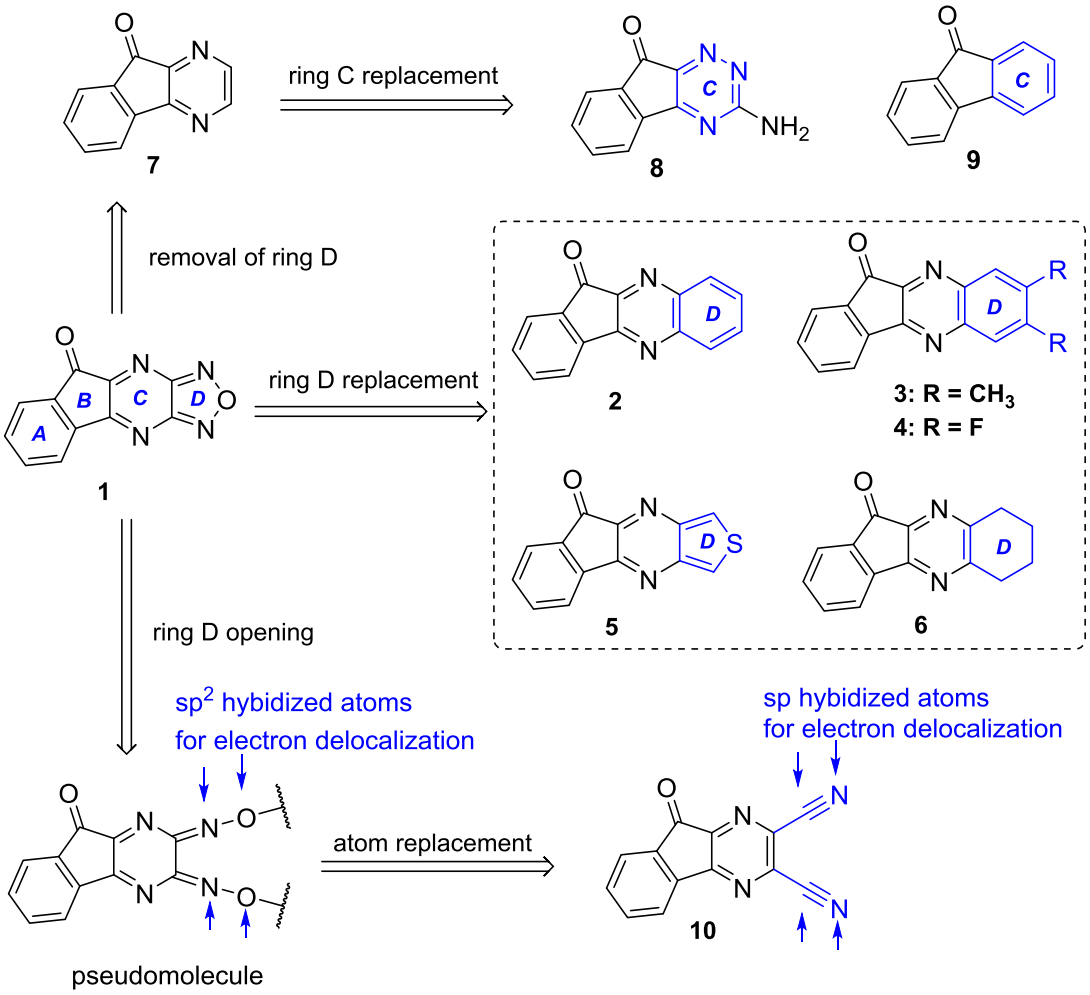

Figure 3. Design of the Target Compounds **2-10** Focusing on the Rings C and D of **1**.

Table 1. Reduction rates of the Target Compounds **1-10** Catalyzed by NQO1.

compd	reduction rate by NQO1 (μmol NADPH/min/μmol NQO1)	N (cycles) [a]
1	1412 ± 64	23
2	362 ± 30	5
3	300 ± 22	5
4	320 ± 35	4
5	316 ± 21	4
6	254 ± 34	4
7	356 ± 41	5
8	347 ± 65	5
9	NA [b]	–
10	1362 ± 38	20
β-lap	1155 ± 44	20

[a] The equiv of NADPH utilized relatives to the equiv of substrates over the course of the assay (in 5 min).
[b] No activity.

*SAR Studies Focusing on Rings B and C of Tricyclic Compound **10***. Next, for further exploring the SAR, the target compounds **11-19** focusing on Rings B and C of **10** were designed as illustrated in Figure 4. Their reduction rates and N (cycles) by NQO1 were determined, and the results were shown in Table 2. Removal of the carbonyl group in B ring as in **11** led to a complete loss in activity, suggesting that the carbonyl group was crucial for NQO1 reduction. Compounds **12-16** were designed by replacing the cyano group at C3 with groups containing lone pair electrons, such as oxygen-containing compounds **12-13**, nitrogen-containing compounds **14-15**, and halogen-containing compound **16**. However, compounds **12-16** showed extremely low reduction rates ranging from 117 to 260 μmol NADPH/min/μmol NQO1 (Table 2). Further, the target compounds **17-19** were generated by changing the linear cyano group into similarly linear alkynyl groups with *sp* hybridized carbon atoms. Nevertheless, they all exerted significantly decreased activity when compared to **10**. In addition, compound **19** with bulky benzyl substitution to the end of alkynyl moiety could hardly be reduced by NQO1. The results demonstrated that the cyano groups substituted at ring C played a crucial role for NQO1 reduction activity and these sites were not suitable for further modification.

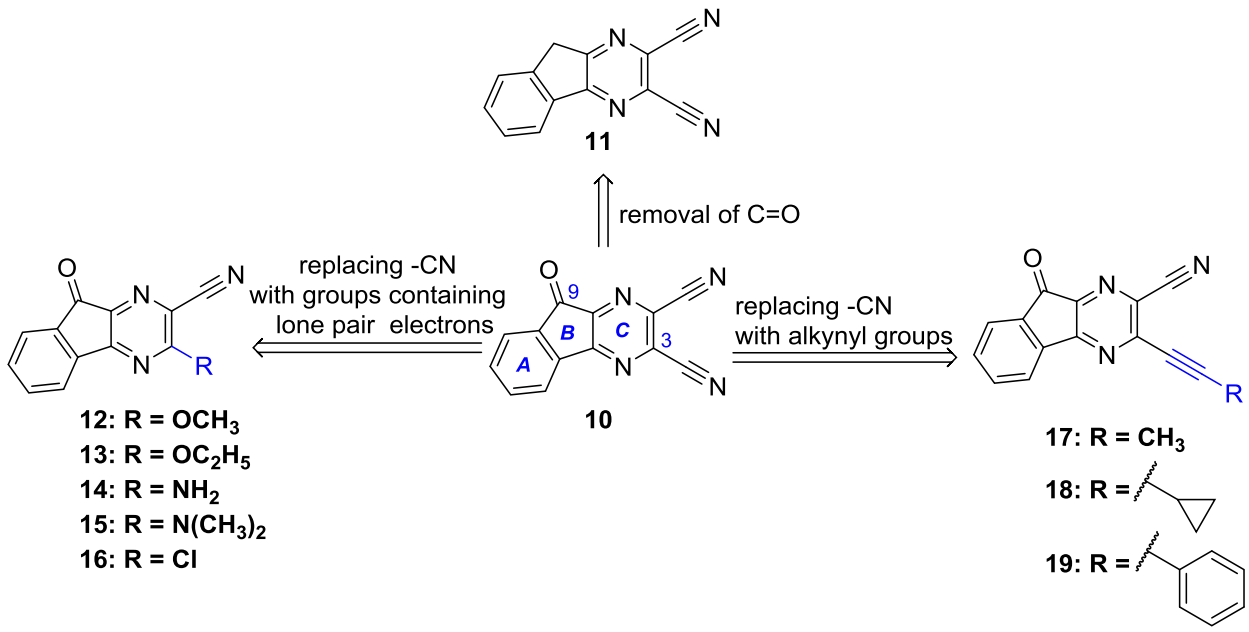

Figure 4. Design of the Target Compounds **11-19** Focusing on the Rings B and C of **10**.

Table 2. Reduction Rates of the Target Compounds **11-19** Catalyzed by NQO1.

compd	reduction rate by NQO1 (μmol NADPH/min/μmol NQO1)	N (cycles) [a]
11	NA [b]	–
12	151 ± 33	2
13	183 ± 42	3
14	149 ± 34	2
15	260 ± 45	4
16	117 ± 30	2
17	332 ± 63	4
18	363 ± 92	5
19	NA [b]	–
10	1362 ± 38	20
β-lap	1155 ± 44	20

[a] The equiv of NADPH utilized relatives to the equiv of substrates over the course of the assay (in 5 min).

[b] No activity.

*SAR Studies Focusing on A Ring of Tricyclic Compound **10***. According to the SAR information above, the following moieties including the carbonyl group in ring B, the nitrogen-containing pyrazine ring C, and the cyano groups substituted on C, were revealed to be important

pharmacorphoric features responsible for **10** by NQO1 reduction. Thus, we retained these features in the subsequent modification and focused on the ring A of **10**. The target compounds **20a-m** were designed by introducing different groups, mainly concerning the electronic effects, such as weak electron-donating group (–CH_3), strong electron-donating groups (–OCH_3 and –OH), and electron-withdrawing groups (F, Cl, and –CF_3) (Table 3). As shown in Table 3, mono-substituted compounds **20a-g** were all efficient NQO1 substrates and redox cyclers, possessing reduction rates ranging from 1104 to 1376 μmol NADPH/min/μmol NQO1 that were comparable to **10**. Interestingly, mono-substitutions with electron-withdrawing groups (-F and –CF_3) as in **20f-g** were found to be more beneficial for improving NQO1 reduction activity as compared to mono-substitutions with electron-donating groups such as –CH_3, –OCH_3, and –OH as in compounds **20a-e**. Further, introducing di-substitutions with electron-donating –CH_3 (**20h**) and –OCH_3 (**20i-j**) significantly led to decrease in reduction rates by NQO1 (656-902 μmol NADPH/min/μmol NQO1) when compared to **10**. Notably, among this series of target compounds, **20k** with difluoro substitution at C6 and C7 sites of ring A revealed to be the most efficient NQO1 substrate with a reduction rate of 1471 ± 42 μmol NADPH/min/μmol NQO1, as well as the most efficient redox cycler, showing 25 redox cycles in the presence of NQO1 in 5 min (Table 3), which was much more efficient than **10** and β-lap. Changing the positions of difluoro groups in **20k** to C5 and C8 as in **20l**, and replacing the difluoro with dichloro groups as in **20m** both resulted in decreased activity when compared with **20k**.

In addition, representative compounds **1**, **10**, **20i**, and **20k** were selected to calculate their catalytic efficiency. The reduction rates by NQO1 at various concentrations (3.1-70 μM) were determined and the corresponding Michaelis-Menten curves were subsequently generated (Figure 5). It was observed that compound **20k** was the most efficient substrate (k_{cat}/K_M = 6.2 ± 1.1 × 10^6

$M^{-1}s^{-1}$), possessing much better kinetic parameters than **10** ($k$cat/K_M = 5.1 ± 0.9 × 10^6 $M^{-1}s^{-1}$) and β-lap ($k$cat/K_M = 4.4 ± 0.9 × 10^6 $M^{-1}s^{-1}$).

Table 3. The Target Compounds **20a-m** Focusing on Ring A of **10**, and Their Reduction Rates Catalyzed by NQO1.

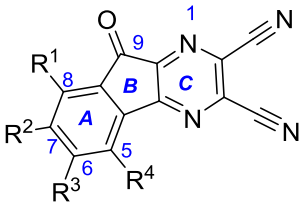

20a-m

compd	R^1	R^2	R^3	R^4	reduction rate by NQO1 (μmol NADPH/min/μmol NQO1)	N (cycles) [a]
20a	H	H	CH_3	H	1197 ± 44	20
20b	OCH_3	H	H	H	1298 ± 58	20
20c	H	OCH_3	H	H	1104 ± 43	18
20d	H	H	OCH_3	H	1118 ± 36	18
20e	H	H	OH	H	1141 ± 39	18
20f	H	H	F	H	1376 ± 65	21
20g	H	H	CF_3	H	1365 ± 53	20
20h	H	CH_3	CH_3	H	902 ± 43	12
20i	H	OCH_3	OCH_3	H	656 ± 88	10
20j	OCH_3	H	H	OCH_3	768 ± 78	10
20k	H	F	F	H	1471 ± 42	25
20l	F	H	H	F	1302 ± 69	20
20m	H	Cl	Cl	H	1180 ± 72	18
10	H	H	H	H	1362 ± 38	20
β-lap					1155 ± 44	20

[a] The equiv of NADPH utilized relatives to the equiv of substrates over the course of the assay (in 5 min).

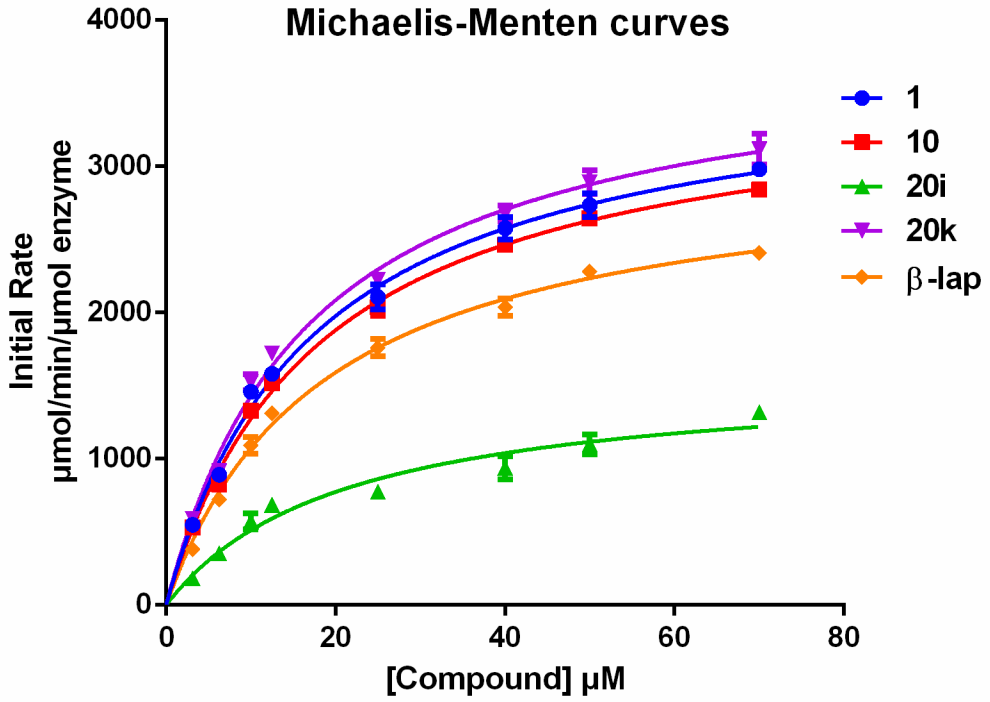

Figure 5. Michaelis-Menten curves for **1, 10, 20i, 20k** and β-lap with NQO1.

Synthesis of the Target Compounds. The target compounds **2-8** and **10** were synthesized using the routes summarized in Scheme 1. Briefly, diverse diamine materials (**22a-c, 23-27**) reacted with ninhydrin hydrate (**21**) in the presence of acetic acid using ethanol as solvent to give efficiently the target compounds **2-8** and **10** in one step. Target compound **9** was commercially available and was purchased directly. The rest target compounds **11-19** and **20a-m** were synthesized using the routes summarized in Scheme 2. Similarly, indanedione **28** reacted with 2,3-diaminomaleonitrile (**27**) in isopropanol at room temperature gave **11** in one step with a yield of 82%. Treatment of **10** with corresponding nucleophiles such as sodium alkoxides and amines gave **12-15** in moderate yields of 37-87%. Compound **16** was synthesized by heating **14** in acetonitrile in the presence of *tert*-butyl nitrite and $CuCl_2$ in 58%. Subsequent treatment of **16** with corresponding alkynes through Sonogashira coupling reaction gave **17-19** in acetonitrile in 24-36%. Compounds **20a-m** were obtained by cyclization of different substituted indanediones (**29a-**

m) with 2,3-diaminomaleonitrile (**27**) in ethanol and followed by oxidation using potassium bichromate in a mixture solvent of acetic acid and water in 42-66% over two steps.

Scheme 1. Synthetic Routes for the Target Compounds **2-8**, and **10**.[a]

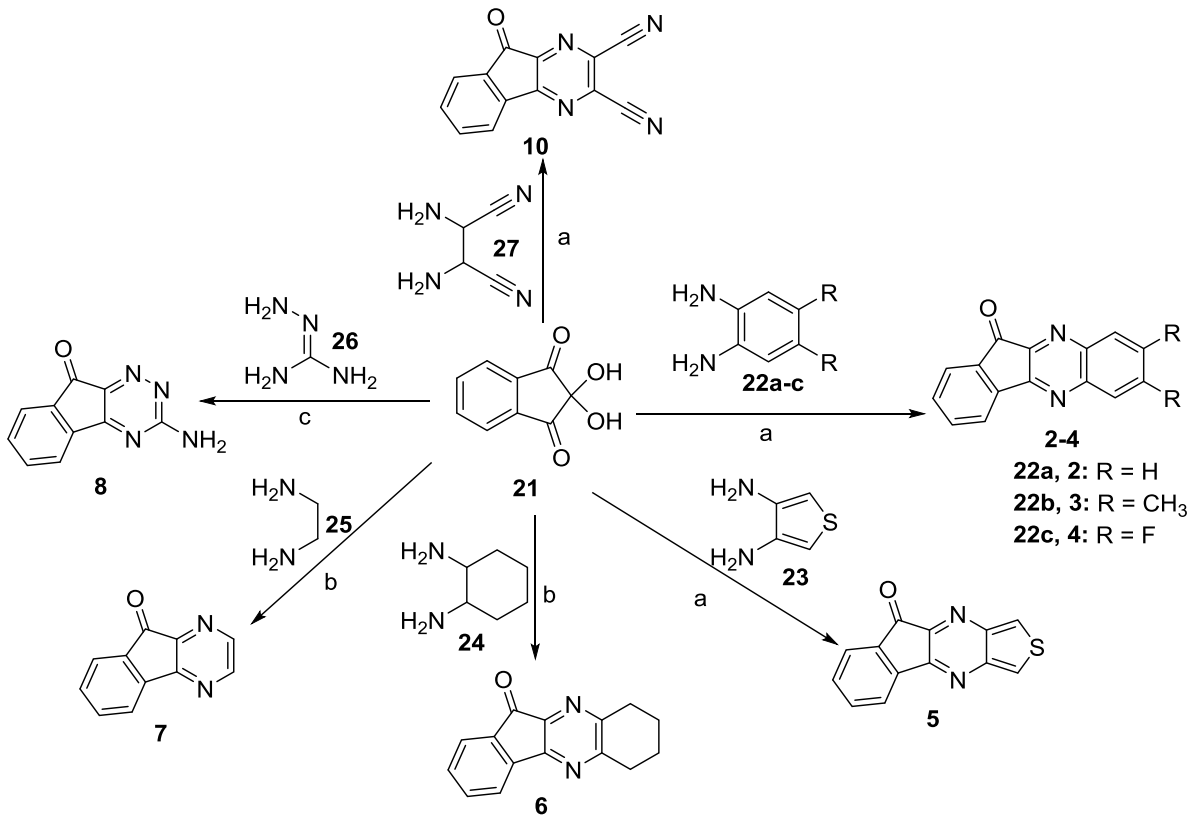

[a] Reagents and conditions: (a) AcOH, EtOH, rt, 2 h, 73-86%; (b) AcOH, EtOH, 40 °C, 4 h, 28-30%; (c) AcOH, EtOH, 70 °C, 4 h, 66%.

Scheme 2. Synthetic Routes for the Target Compounds **11-19**, and **20a-m**.[a]

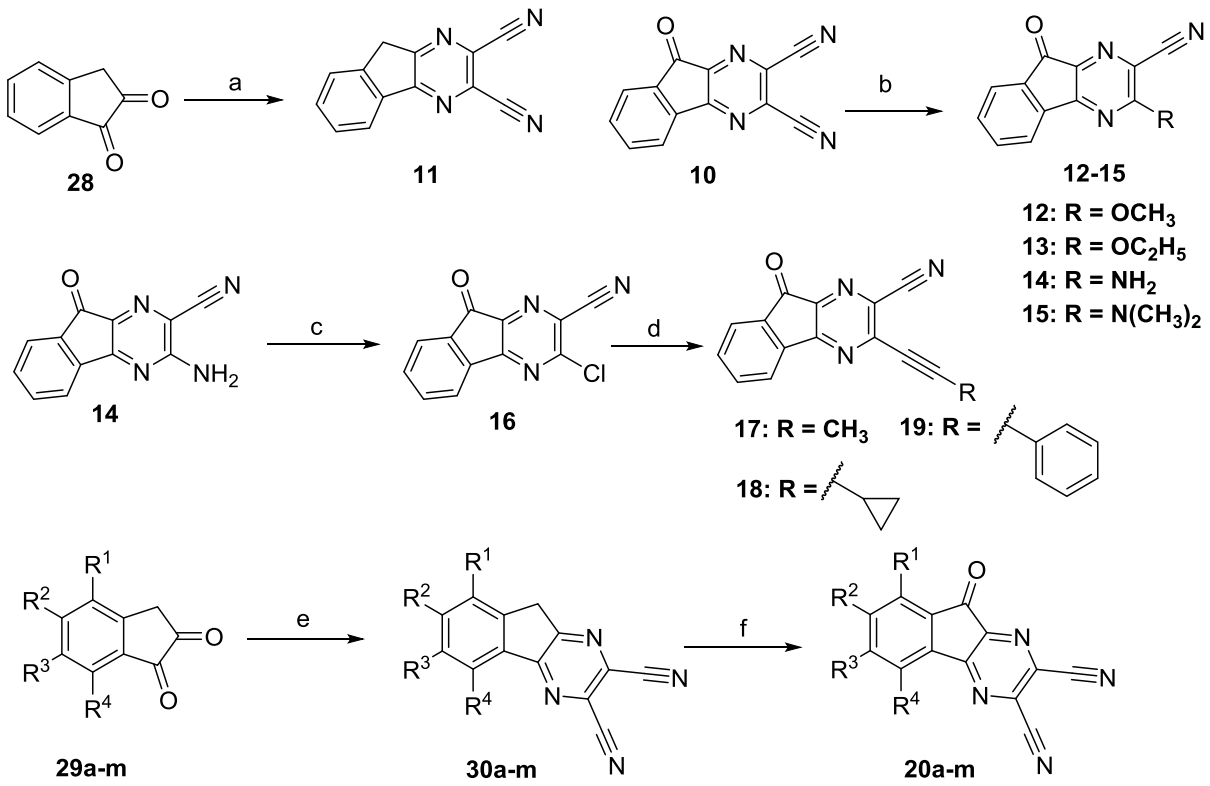

[a] Reagents and conditions: (a) **27** (1 equiv), isopropanol, rt, 2 h, 82%; (b) corresponding sodium alkoxides (1 equiv) or amines (1-3 equiv), THF, rt, 2 h, 37-87%; (c) *tert*-butyl nitrite (5 equiv), $CuCl_2$ (5 equiv), CH_3CN, 65 ^oC, 4 h, 58%; (d) corresponding alkynes (1.5 equiv), $Pd(dppf)_2Cl_2$ (0.1 equiv), CuI (0.1 equiv), Et_3N (1.1 equiv), CH_3CN, 80 ^oC, 3 h, 24-36%; (e) **27** (1 equiv), EtOH, rt, 6 h; (f) $K_2Cr_2O_7$ (0.6 equiv), AcOH, H_2O, 100 ^oC, 1 h, 42-66% over two steps. The detailed R groups for **20a-m** see Table 3.

SAR Analysis by Electrochemical Property. Electrochemistry is the standard method for studying chemical redox reactions, and electrochemical techniques has been considerably applied to biology.[40] We have investigated and reported on the electrochemical behavior of *ortho*-quinones.[41] As for redox cycling substrates for NQO1, undoubtedly, the electrochemical parameters were always correlated with their biological activities. In this work, the electrochemical studies were consequently performed to investigate the electrochemical behavior of the non-quinone redox cycler and to further explain their SAR.

Representative compounds (Figure 6) were selected to contain each of the structural classes. The E_{redox} values, with reference to ferrocene ($F_c^{0/+}$), were determined and shown in Figure 6 and the cyclic voltammograms (CV) of the representative compounds were shown in Figure S2.

As illustrated in Figure 6, these investigated non-quinone compounds possessed E_{redox} values in the range of -0.918 V to -1.500 V. It has been suggested that the E_{redox} values of successful NQO1 quinone substrates should be in the range of -0.70 V to -1.20 V, and the compounds were hard to be bioreduced by NQO1 if the E_{redox} values were beyond the range.[42] The non-quinone compounds with an indenopyrazinone scaffold in this work were also found to meet the requirement of the rule. Compounds (**20k**, **1**, and **10**) with rapid NQO1 reduction rates (> 1300 μmol NADPH/min/μmol NQO1) showed higher E_{redox} values (> -0.1V) ranging from -0.918 V to -0.994 V, while compounds (**12**, **7**, **17**, and **2**) with very slow NQO1 reduction rates exhibited much lower E_{redox} values (< -1.2 V). These results could well explain why the replacement by a benzene ring (as in **2**) or removal of ring D (as in **7**) of compound **1**, and changing of the cyano group of compound **10** (as in **12** and **17**) were all detrimental for reduction by NQO1. Furthermore, compound **20k**, which was derived by introducing additional electron-withdrawing difluoro substituents to **10**, exerted a slightly increased E_{redox} value, resulting in improvement of NQO1 reduction rate when compared to **10**. Similarly, in the case of **20i**, possessing additional electron-donating methoxy groups, led to a decrease in E_{redox} value and a significant decline in NQO1 reduction activity. In summary, as for the non-quinones with an indenopyrazinone scaffold in this work, the electrochemical reduction potentials could correlate well with their reduction rates by NQO1, and the preferable E_{redox} values fell within -0.70 V and -1.0 V. These findings provided us a complementary method to further design and optimization of this new chemotype of redox cycling substrates by NQO1 for developing novel ROS generating antitumor agents.

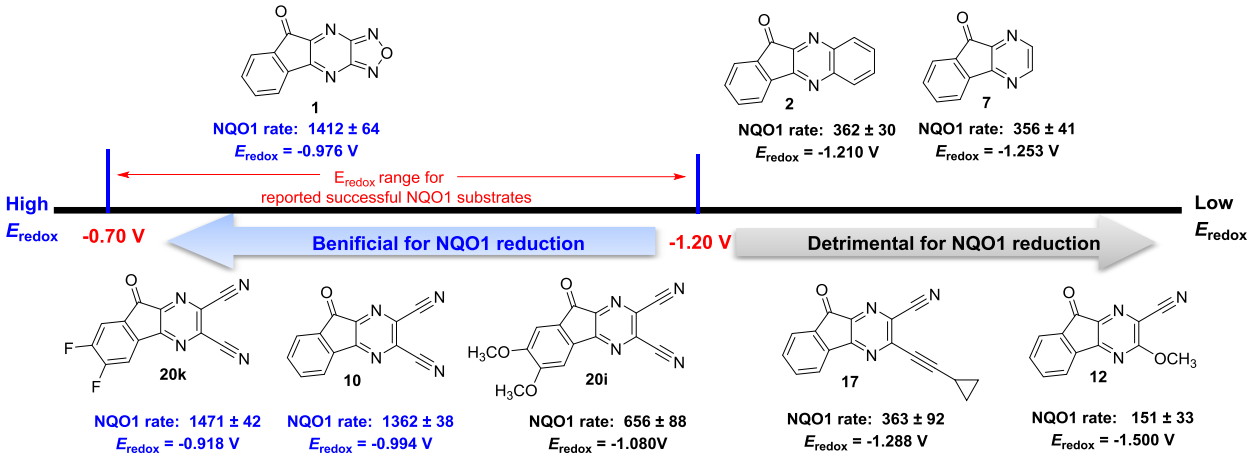

Figure 6. E_{redox} values and NQO1 rates for representative target compounds.

Binding Mode and Catalytic Analysis by Molecular Modelling. Utilizing the crystal structure of NQO1 (PDB ID: 1H69),[43] molecular modelling was performed using GOLD 5.1 software[44] and depicted using PyMOL to elucidate the possible binding mode of NQO1 with tetracyclic hit compound **1** (Figure 7A) and the most active, representative tricyclic compound **20k** (Figure 7B), and the other compounds used in electrochemistry study (Figure S3). It was shown that they lay deep into the catalytic sites of NQO1 protein and was oriented above the isoalloxazine ring of bound cofactor FAD by π-stacking interaction. This was similar to the reported quinone substrates.[45] The carbonyl group and N1 atom of **1** and **20k** could interact with the Tyr126 and Tyr128 residues by hydrogen bonding, respectively (Figure 7A and 7B). The residues including Trp105, Phe106, and Phe178 formed a hydrophobic pocket of sufficient size to allow only small substituents to interact favorable. Besides of matching for the catalytic binding site of NQO1, the substrates to be bioreduced by NQO1 required an appropriate hydride donor-acceptor distance between the acceptor site in substrate and the FAD cofactor (atom N5 which transfer the hydride) in NQO1.[46] Thus, the distance between the carbon atom of C(9)=O in **20k** and the nitrogen atom of N(5)H in FAD was calculated as 3.425 Å, which was within a reasonable distance (<4 Å) for

hydride transfer, the key process for initiating NQO1 bioreduction. Based on this, the catalytic process for the reduction of the new chemotype of non-quinone substrates by NQO1, as exemplified by **20k**, was proposed as illustrated in Figure 7C. The C(9)=O moiety acted as a electrophilic site for accepting hydride (H^-) from the reduced FAD ($FADH_2$), which is similar to that of quinone substrate β-lap (Figure S4). The two hydrogen bonding interaction of C(9)=O…Tyr126 and N(1)….Tyr128 were suggested to reduce the electron density of the C9 hydride acceptor, thus facilitating hydride (H^-) transfer from $FADH_2$. Meanwhile, the Tyr126 and Tyr128 residues were also responsible for promoting substrate **20k** (oxidized form) to accept another proton (H^+), thus completing the reduction process to give **20k-H2** (reduced form). Notably, it is the N(1) atom that plays as the proton acceptor in nonquinone substrate **20k,** while it is the C=O moiety in quinone substrate β-lap (Figure S4). These computational findings were also in accordance with the key pharmacophoric features aforementioned. In addition, the efficient recovery of substrate **20k** after NQO1-mediated redox cycling has also been observed experimentally in an HPLC-based assay (Figure S5).

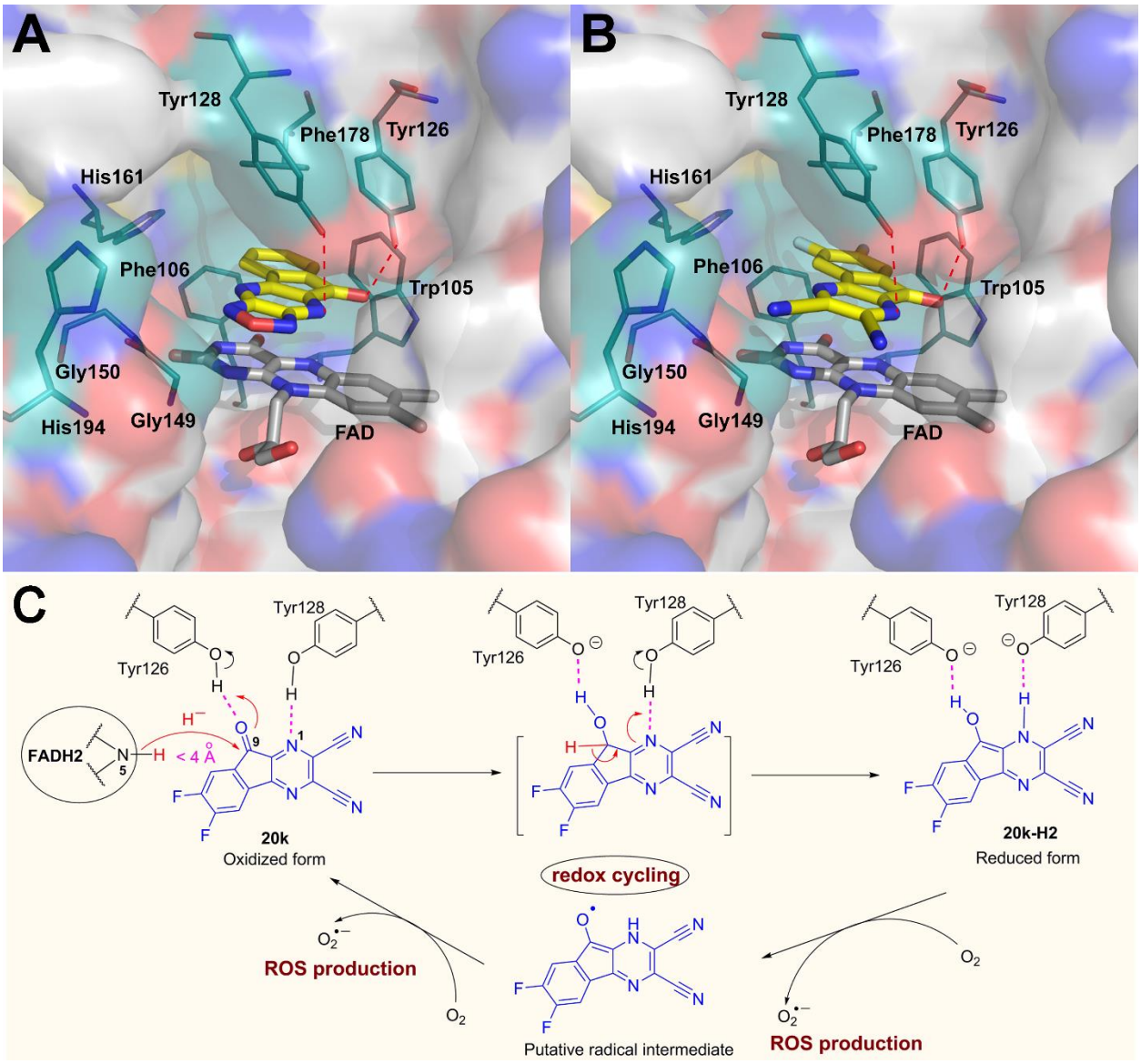

Figure 7. Docked poses of compounds **1** (A) and **20k** (B) into the catalytic sites of NQO1 (PDB code: 1H69). (C) Proposed redox cycling process for **20k** by NQO1 reduction.

2.3. In Vitro Antitumor Evaluation. On the basis of the enzymatic assays and electrochemical studies, compounds (**1**, **10**, and **20a-20m**) that possessed good NQO1 reduction rates and preferable redox cycling properties, were selected for cellular assays to investigate their potency against NQO1-rich NSCLC cells (A549 cells and Taxol-resistant A549/Taxol cells) and

NQO1-deficient normal hepatic cells (L02) by the MTT assay. β-Lap and Taxol were used as comparison controls. As shown in Table 4, all the target compounds were sensitive to NQO1-rich and Taxol-resistant A549/Taxol cancer cells with IC_{50} values ranging from 0.6 to 6.8 μM, which were much more potent than Taxol (IC_{50} = 27.0 μM). These compounds were also active to NQO1-rich A549 cancer cells with IC_{50} values ranging from 0.8 to 5.9 μM. Whereas in the case of NQO1-deficient normal L02 cells, the compounds were much less sensitive, exerting IC_{50} values ranging from 14.3 to 35.9 μM, showing a desirable selectivity between cancer and normal cells. Notably, all of the tricyclic target compounds (**10** and **20a-m**) were less toxic to normal L02 cell when compared to the tetracyclic hit **1**. Relative high selectivity ratios in compounds **20f** and **20k-m** were observed, being much greater than hit **1** and positive control β-lap. Interestingly, these compounds with high selectivity were found to be substituted with fluoro or chloro in the ring A. Among all the compounds tested, **20k**, the most excellent redox cycling substrate for NQO1, turned out to be the most active and selective tricyclic non-quinone compound to drug resistant A549/Taxol cancer cells with an IC_{50} value of 0.6 μM and a selectivity ratio of 50.3. Besides, as shown in Figure 8, **20k** was also found to be active toward other NQO1-overexpressing human cancers (Figure S1) such as multidrug resistant A549/VCR lung cancer cells, MCF-7 breast cancer cells, and MIA PaCa-2 pancreatic cancer cells. As for NQO1-deficient human lung cancer H596 cells, **20k** was much less sensitive (Figure 8).

In addition, when the A549/Taxol cells were pretreated with either 50 μM dicoumarol (DIC) as a NQO1 inhibitor or 10 mM *N*-acetylcysteine (NAC) as an antioxidant prior to treatment with **20k**, compound **20k** exhibited a 42 to 55-fold less antiproliferative activity against A549/Taxol cells (A549 + DIC and A549 + NAC, IC_{50} = 25.6 μM and 33.2 μM, respectively) (Figure 9). The

results indicated that **20k** exhibited antitumor activity and overcame drug resistance through NQO1-dependent and ROS-mediated pathways.

Table 4. Cytotoxicity of Representative Non-Quinone Compounds toward NQO1-Rich A549 and A549/Taxol Cancer Cells, and NQO1-Deficient L02 Normal Cells.

compd	cytotoxicity IC_{50} (μM)			selectivity ratio IC_{50} (L02)/ IC_{50} (A549/Taxol)
	A549/Taxol (NQO1-rich)	A549 (NQO1-rich)	L02 (NQO1-deficient)	
1	0.6 ± 0.1	1.0 ± 0.2	14.3 ± 1.6	23.8
10	2.9 ± 0.1	1.4 ± 0.3	21.3 ± 1.8	7.3
20a	2.7 ± 0.3	1.5 ± 0.3	26.0 ± 1.5	9.6
20b	2.4 ± 0.3	0.8 ± 0.2	22.6 ± 1.6	9.4
20c	4.9 ± 0.1	2.3 ± 0.5	21.6 ± 1.3	4.4
20d	2.2 ± 0.7	2.1 ± 1.5	22.0 ± 2.4	10.0
20e	6.7 ± 0.6	3.5 ± 0.8	25.0 ± 1.4	3.7
20f	0.8 ± 0.2	1.4 ± 0.4	26.1 ± 0.8	32.6
20g	4.1 ± 1.5	5.2 ± 1.0	28.8 ± 2.3	7.0
20h	6.3 ± 0.6	4.4 ± 0.5	30.9 ± 1.4	4.9
20i	5.1 ± 0.2	4.5 ± 1.2	28.1 ± 0.8	5.5
20j	6.8 ± 0.1	5.9 ± 0.4	35.9 ± 0.9	5.3
20k	0.6 ± 0.1	1.0 ± 0.3	30.2 ± 1.3	50.3
20l	0.9 ± 0.2	1.9 ± 0.3	23.0 ± 1.2	25.6
20m	1.3 ± 1.5	2.7 ± 1.0	35.8 ± 2.3	27.5
Taxol	27.0 ± 1.6	0.7 ± 0.2	5.6 ± 2.1	0.2
β-lap	1.9 ± 0.5	3.1 ± 0.8	11.9 ± 1.4	6.3

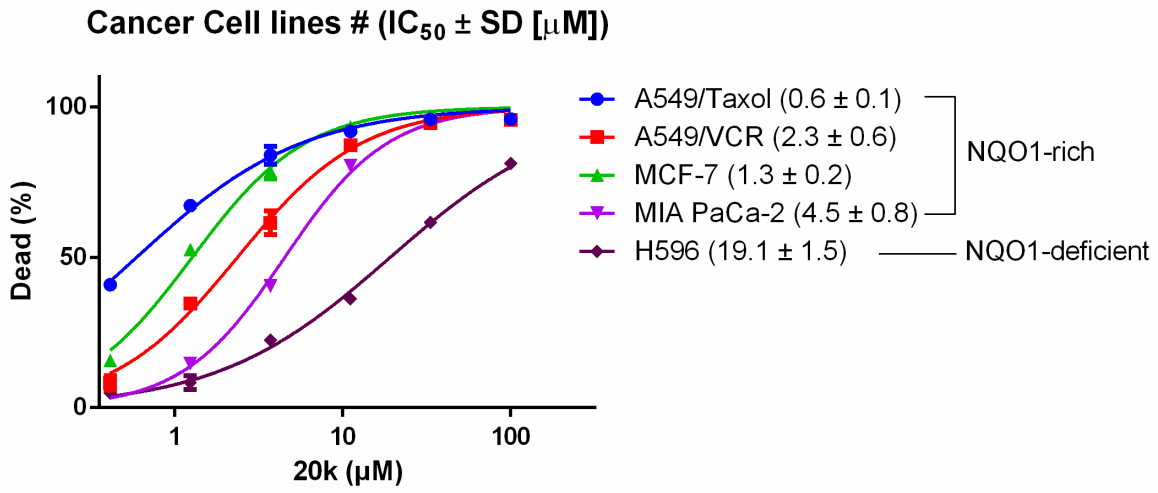

Figure 8. Cytotoxicity of **20k** toward NQO1-rich A549/Taxol, A549/VCR, MCF-7, and MIA PaCa-2 cancer cells and NQO1-deficient H596 lung cancer cells.

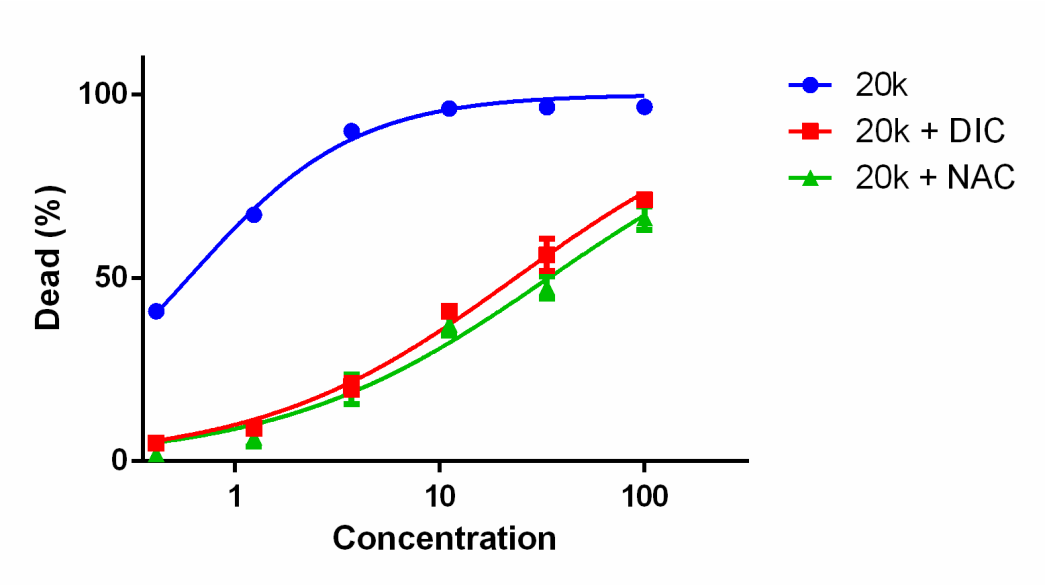

Figure 9. Cytotoxicity of **20k** toward A549/Taxol cancer cells in the presence and absence of the NQO1 inhibitor (DIC, 50 μM) and ROS Scavenger (NAC, 10 mM).

2.4. Determination of ROS Generation in Cell-Free and Cell-Based Assays. *Determination of ROS Generation in a Cell-Free Assay.* Considering that the redox cycling could lead to rapid ROS generation, we thus selected representative compounds (**1**, **10**, and **20k**) with efficient NQO1 reduction rates to further identify their abilities to generate ROS. Compound **20k** coincubated with NQO1 inhibitor DIC, and compounds **9** and **11** with no NQO1 reduction activity were selected as negative controls. β-Lap was chosen as a positive control. The production of superoxide anion, the main constitute of ROS, was measured by a cell-free spectrophotometric assay using cytochrome c as the terminal electron acceptor. As shown in Figure 10, the non-quinones **1**, **10**, and **20k** showed rapid rates of ROS generation, being much more efficient than β-lap. Compound **20k** with the highest metabolic rate by NQO1 (1471 ±42 μmol NADPH/min/μmol NQO1) (Table 3) also exhibited the highest rate of ROS production (1208 ±45 μmol cyt c/min/mg NQO1) (Figure 10). Further, coincubation with DIC dramatically reduced the rate of ROS

production by **20k**. In addition, compounds **9** and **11** without NQO1 reduction activity also failed to generate ROS by NQO1.The results indicated that these non-quinone substrates could rapidly generate a high level of ROS through NQO1-dependent redox cycling.

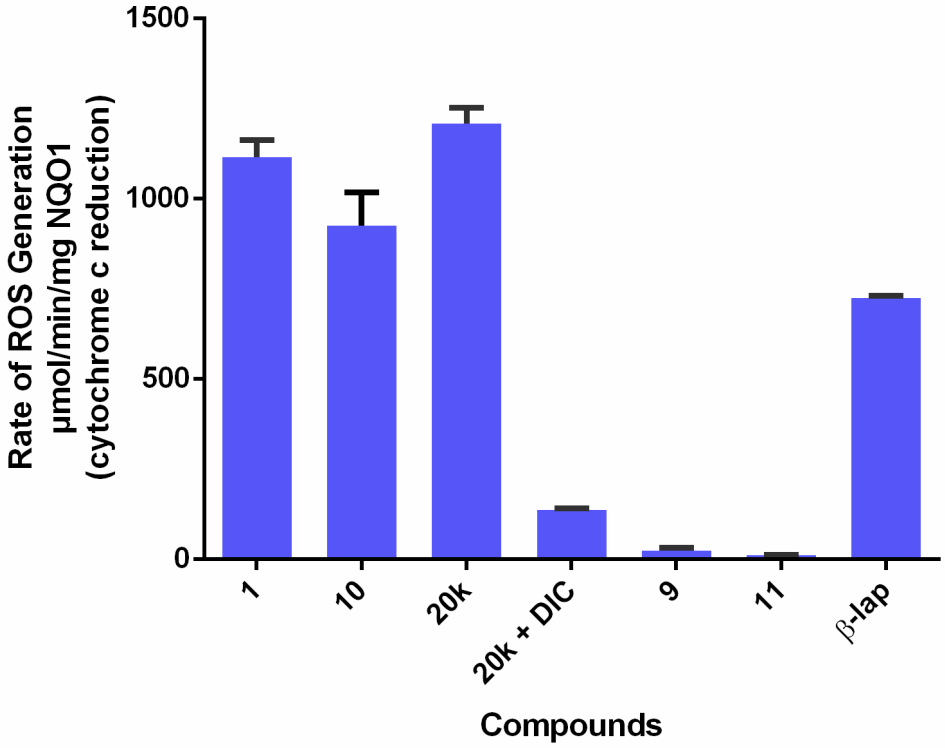

Figure 10. Rate of ROS production of representative compounds (**1**, **10**, and **20k**), **20k** + NQO1 inhibitor DIC (25μM), **9**, and **11** were used as negative controls. β-Lap was used as a positive control.

*Determination of ROS Generation Induced by **20k** in A549/Taxol Cells.* It was supposed that **20k** exerted its antitumor activity by generating ROS through futile redox cycles catalyzed by intracellular NQO1. We then monitored intracellular ROS level using a ROS-sensitive fluorogenic dye (2′,7′-dichlorodihydrofluorescein diacetate, DCFH-DA) after treating the A549/Taxol cells with compounds **20k** and β-lap at 1 and 10 μM for 3 h. As shown in Figure 11A, **20k** strongly

generated excessive ROS in A549/Taxol cells and the ROS levels were even higher than the control β-lap in A549/Taxol cells. Considering that DCFH-DA detects a broad range of ROS including hydrogen peroxide, hydroxyl radical, and peroxy radicals, subsequently, we employed two other ROS sensors that probe more specific ROS in cells. APF (3′-(p-aminophenyl) fluorescein) mainly senses hydroxyl radical, whereas dihydroethidium (DHE) selectively detects superoxide anion in cells.[47,48] Fluorescence imaging with the three different ROS probes showed **20k** generated excessive ROS that mainly included superoxide anion rather than hydroxyl radical (Figure 11B). Notably, the level of ROS generated by **20k** outcompeted that induced by β-lap. When we pretreated the A549/Taxol cells with either 50 μM DIC as a NQO1 inhibitor or 10 mM NAC as an antioxidant prior to treatment with the compound **20k** (10 μM), ROS generation was greatly attenuated. The results indicated that **20k** induced ROS generation in an NQO1-dependent manner in A549/Taxol cells.

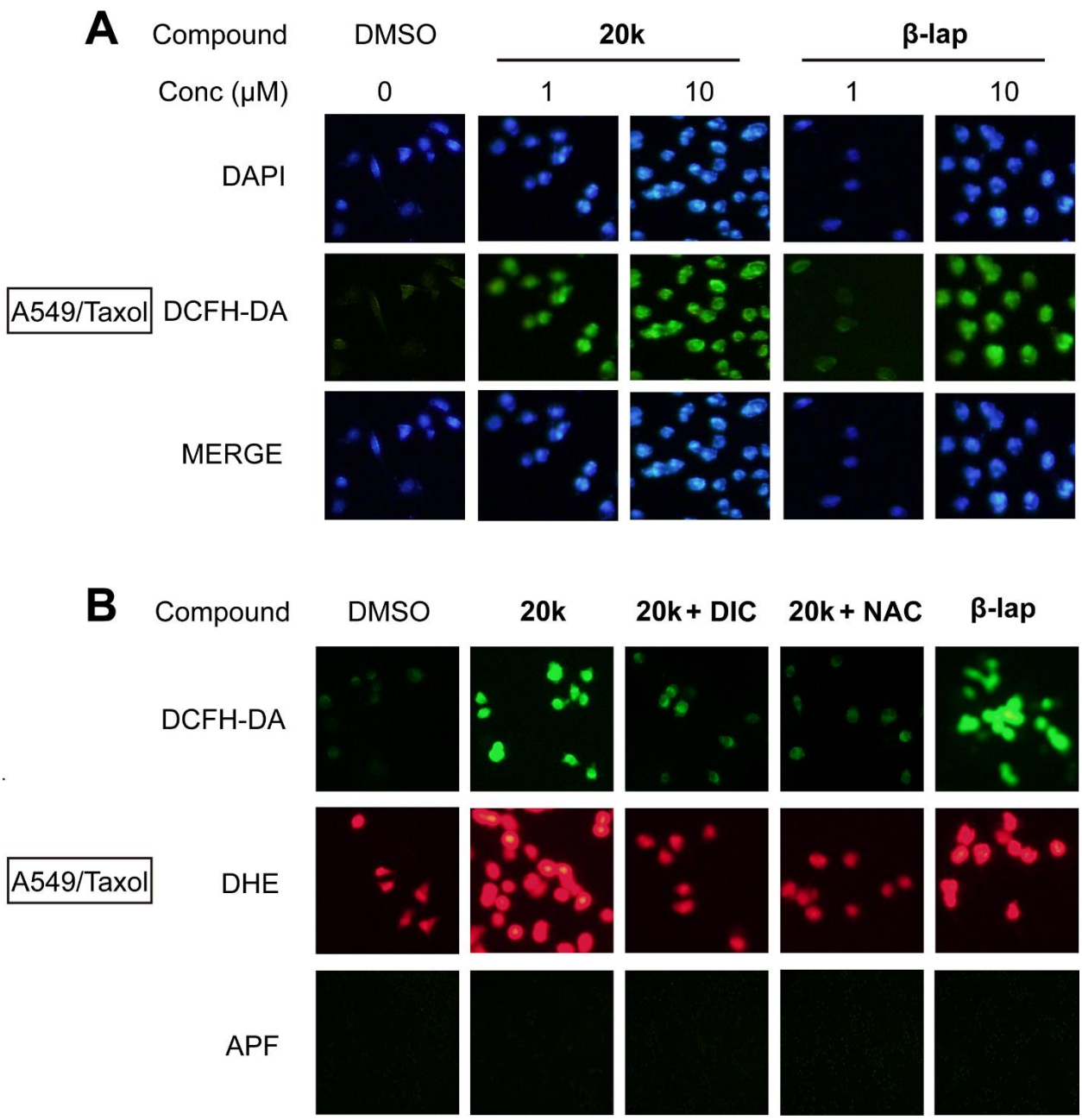

Figure 11. (A) Compound **20k** generated high levels of ROS in A549/Taxol cancer cells. Fluorescence was detected using a fluorescence microscope. (B) Similar experiments were done in A549 cells using three different ROS probes (DCFH-DA, DHE, APF) with pretreatment with 50 μM DIC or 10 mM NAC.

2.5. Pharmacological Studies on Compound 20k in A549/Taxol Cells. *Induction of DNA Damage in A549/Taxol Cells by **20k***. Dramatic ROS induction by **20k** suggested that **20k** exposure may cause damage and breaks in DNA. DNA damage, measured by comet tail formation, was detected in A549/Taxol cells after the treatment with **20k** (10 μM, 2 h) (Figure 12A and 12B), which was comparable to the positive control H_2O_2 (2 mM). Furthermore, DNA damage was greatly attenuated in DIC and NAC pretreated A549/Taxol cells. Thus, the results demonstrated that NQO1-mediated ROS formation by **20k** led to significant DNA breaks.

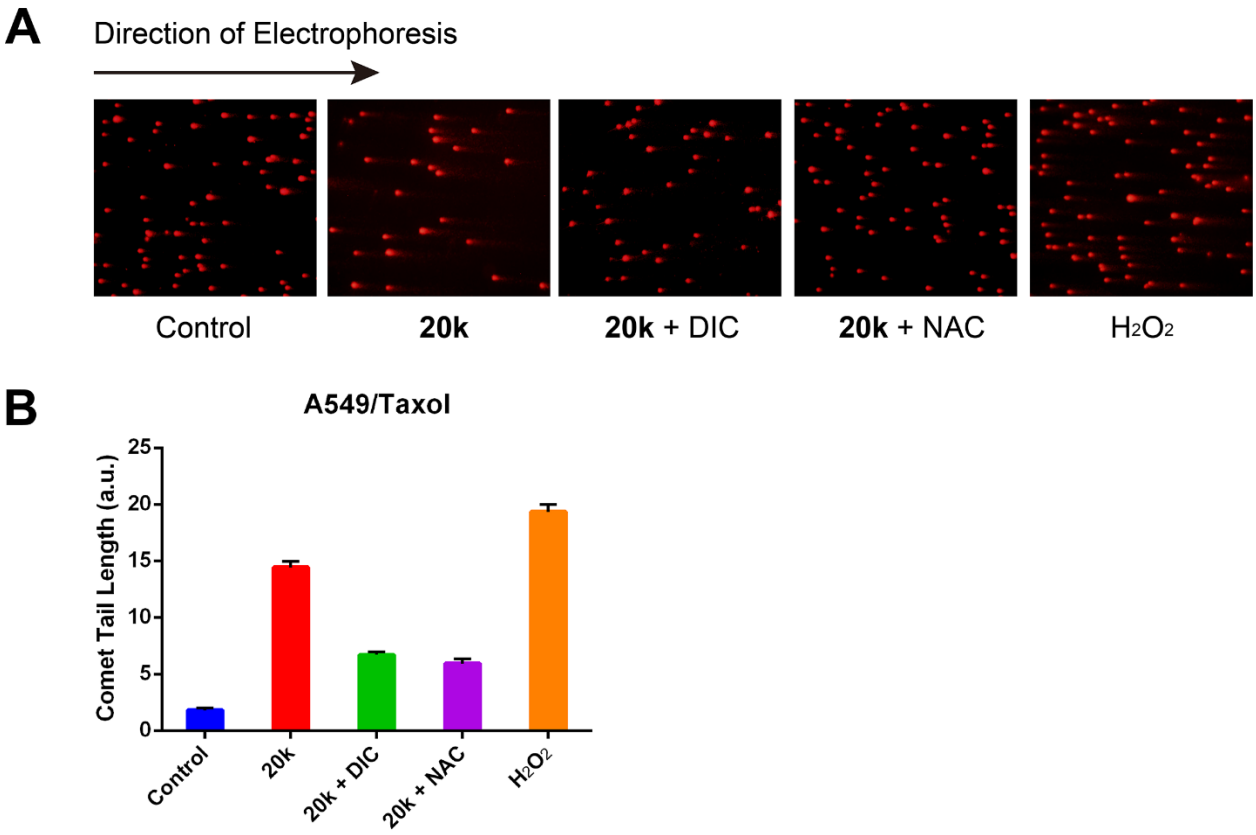

Figure 12. Compound **20k** induced DNA damage in A549/Taxol cells in a NQO1, ROS-dependent manner. Cells were also exposed to 2 mM H_2O_2 for 2 h as positive controls. Comet tail lengths of A549/Taxol cells were measured by using Image J software (a.u., arbitrary unit).

*Effect of **20k** on Nucleotides Depletion by PARP-1 Hyperactivation.* Excessive ROS production and significant DNA breaks were observed after the treatment with **20k** in A549/Taxol cells. Poly(ADP-ribose)polymerase-1 (PARP-1), a critical DNA repair enzyme, is immediately activated after genotoxic stress and catalyze the formation of short-lived negatively charged Poly(ADP-ribose) (PAR) polymers. we examined the role of this repair protein in **20k**-induced lethality. PAR accumulation, an indicator of PARP-1 hyperactivation, was detected in the A549/Taxol cells in 10 min of the treatment of **20k**, then reduced rapidly in a time-dependent manner and disappeared after 60 min of the treatment (Figure 13A). Furthermore, PAR accumulation was suppressed in DIC and NAC pretreated A549/Taxol cells (Figure 13A).

In addition, rapid PAR formation correlated well with loss of essential metabolic nucleotides (i.e., ATP and NAD^+) in the A549/Taxol cells (Figure 13 and 14). Addition of DIC and NAC prevented **20k**-induced PAR formation (Figure 13A) as well as nucleotide loss (Figure 13B). Inhibition of PARP-1 activity using 3-aminobenzamide (3-AB), an NAD^+ analog, spared A549/Taxol cells from **20k**-induced dose-dependent PAR formation (Figure 14A) and attenuated nucleotide depletion (Figure 14B). Thus, PARP-1 inhibition protected cells from **20k**-induced PARP-1 hyperactivation. These results indicated that **20k** induced PARP-1 hyperactivation and depletion of essential nucleotides in an NQO1- and ROS- dependent manner.

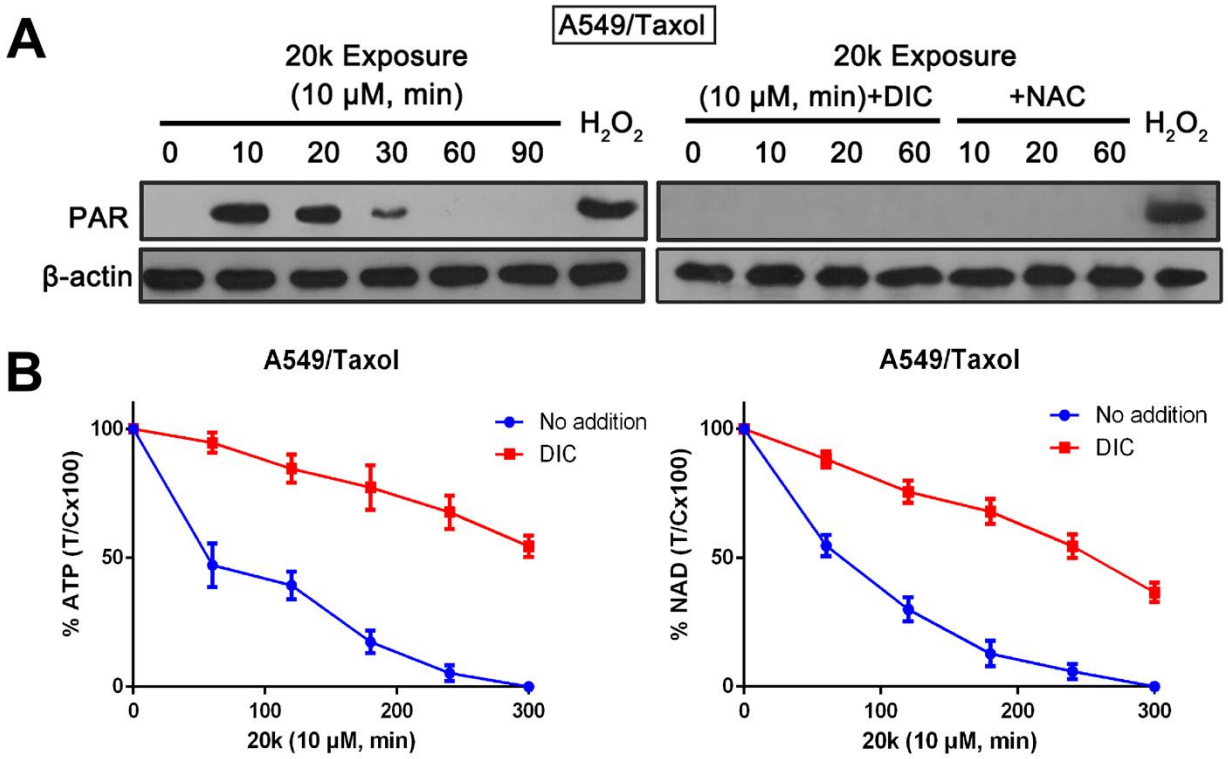

Figure 13. Compound **20k** induced PARP-1 hyperactivation causing NQO1-dependent nucleotide depletion. Cells were exposed to 10 μM **20k** with or without 50 μM DIC and 10 mM NAC, and harvested at the indicated times. (A) Western blot analyses of PAR formation in A549/Taxol cells exposed to compound **20k** (10 μM) (A Left) with or without 50 μM DIC and 10 mM NAC (A Right) and harvested at the indicated times. (B) Changes of intracellular ATP level (A Left) and NAD^+ level (A Right) in the presence and absence of the NQO1 inhibitor (DIC, 50 μM).

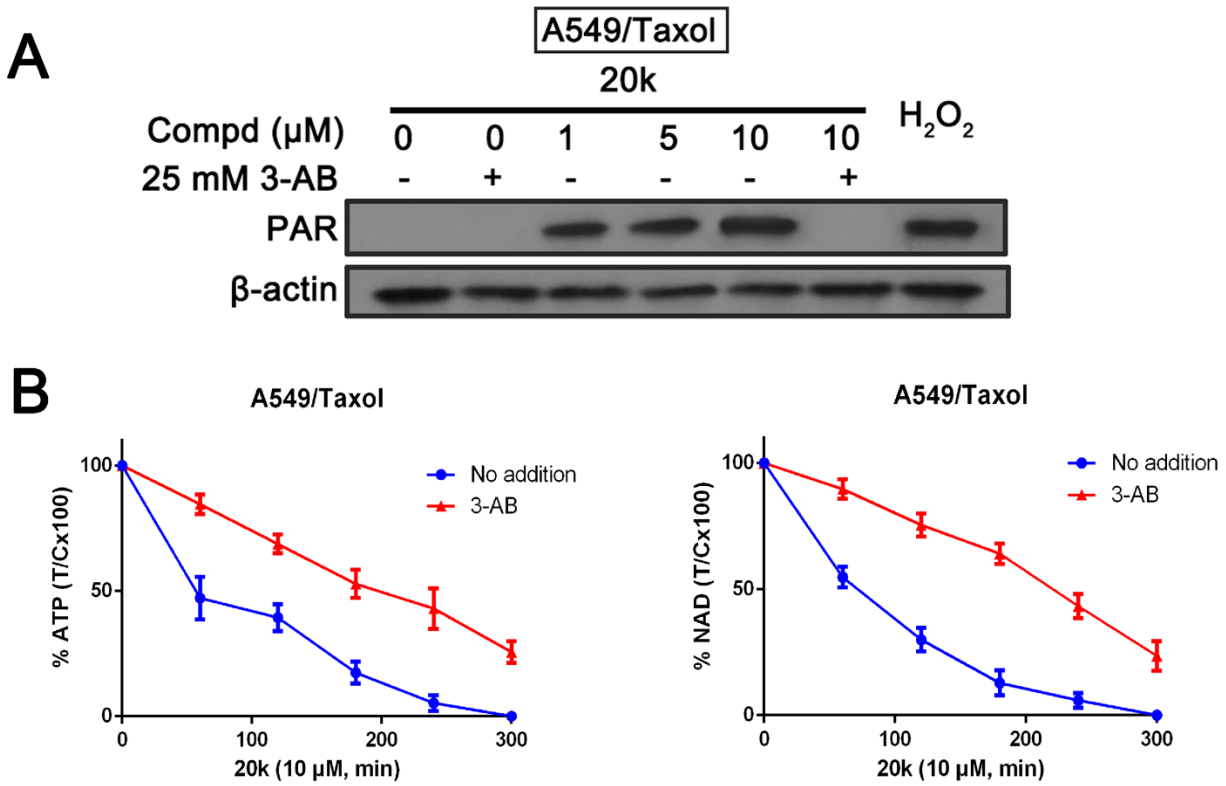

Figure 14. Inhibition of PARP-1 hyperactivation delays NQO1-dependent nucleotide pool depletion in A549/Taxol cells after **20k** treatment. (A) Western blot analyses of PAR formation in A549/Taxol cells exposed to compound **20k** (10 μM) (A Left) with or without 25 mM 3-AB and harvested at the indicated times. (B) Changes of intracellular ATP level (A Left) and NAD^+ level (A Right) in the presence and absence of the PARP-1 inhibitor (3-AB, 25 mM).

*Induction of A549/Taxol Cell Apoptosis by **20k***. To determine whether the inhibitory effects of **20k** on drug resistant lung cancer cellular proliferation are accompanied by enhanced cancer cell apoptosis, Annexin V-FITC and propidium iodide (PI) staining were carried out and the percentages of apoptotic cells were tested using flow cytometry assay. A549/Taxol cells were incubated with different concentrations of **20k** (1, 5, and 10 μM) for 24 h. We observed that treatment with **20k** induced apoptosis in the A549/Taxol cells in a dose-dependent manner, which

was significantly attenuated in DIC and NAC pretreated A549/Taxol cells (Figure 15A and 15B). The results indicated that **20k** induced apoptosis through NQO1-dependent and ROS-mediated pathways.

Furthermore, Western blot analysis showed that **20k** increased the levels of apoptotic markers,[31] including cleaved PARP and p53, in a dose-dependent manner. Likewise, pretreatment with 50 μM DIC and 10 mM NAC attenuated the escalation of cleaved PARP and p53 (Figure 15C), indicating that **20k** induced apoptosis through NQO1-mediated ROS generation.

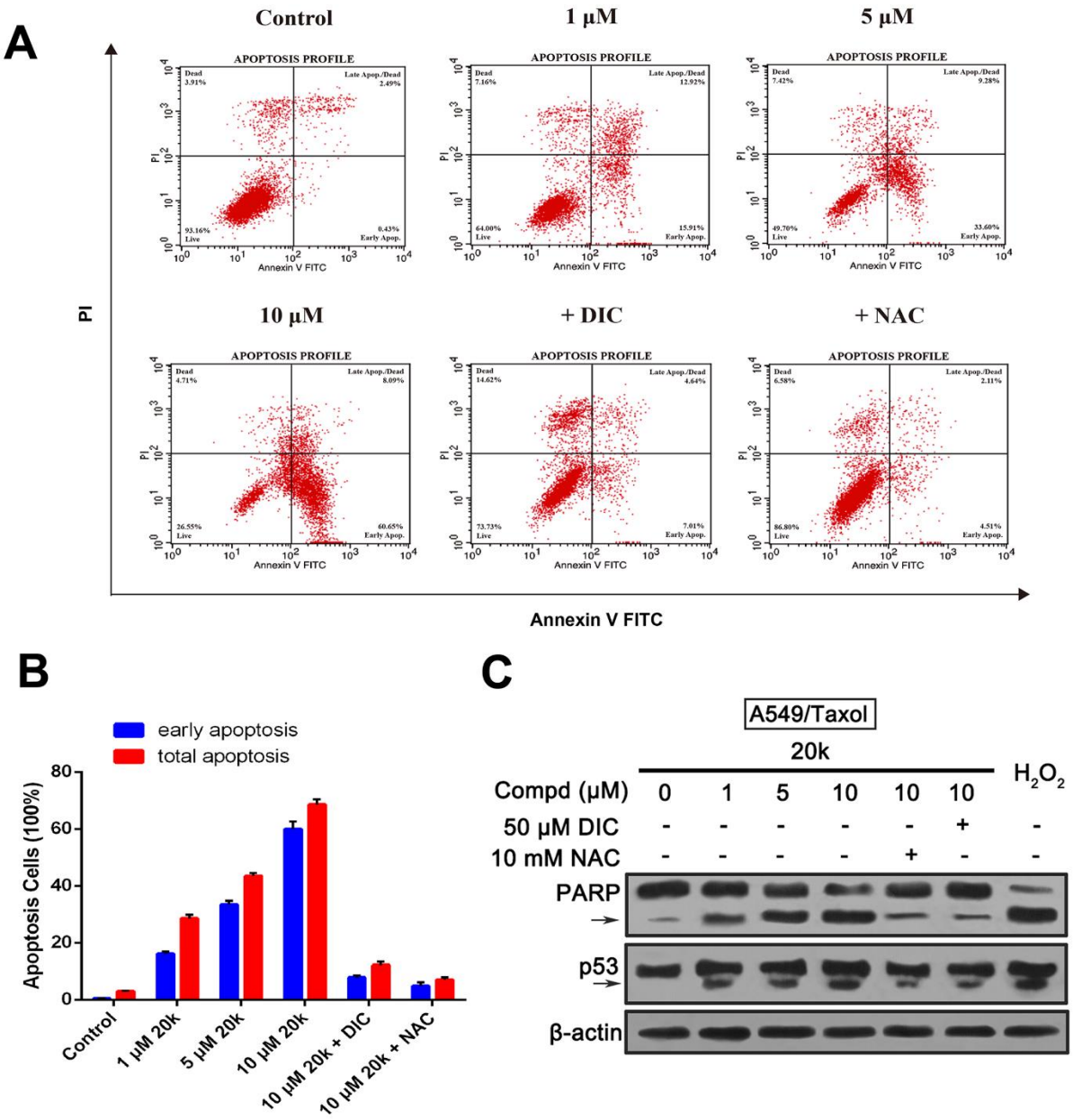

Figure 15. Compound **20k** induced NQO1-dependent apoptosis in A549/Taxol cells. Cells were exposed to 10 μM compound **20k** with or without 50 μM DIC and 10 mM NAC, and harvested at the indicated times. (A) FACS analysis showed apoptosis in A549/Taxol cells after treatment of **20k** for 24 h. (B) Percentage of apoptosis cells after treatment with indicated concentration of **20k**. (C) **20k** blocked the generation of PARP cleavage and p53 in A549/Taxol cells in an NQO1- and ROS-dependent manner. The arrows indicate cleaved PARP and P53, respectively.

2.6. In Vivo Pharmacological Studies on Compound 20k. *Antitumor Efficacy of **20k** in inhibiting the growth of A549/Taxol xenograft tumors in mice*. Compound **20k** was investigated for its in vivo antitumor efficacy against A549/Taxol xenografts. In the study, compound **20k** was administered through tail intravenous injection at 15 mg/kg and 30 mg/kg every other day for three weeks. Taxol (2 mg/kg) was chosen as the reference. As shown in Figure 16, compound **20k** significantly inhibited the growth of A549/Taxol tumor. The T/C values of the 15 and 30 mg/kg doses were 62.1% and 25.9%, respectively (Figure 16A). Meanwhile, the tumor weights of mice treated with **20k** at 30 mg/kg (0.50 $\pm$0.07 g) were reduced by 64.9% as compared with the control (1.43 $\pm$0.15 g) (Figure 16B). In addition, compound **20k** was well tolerated, no significant body weight loss was observed in **20k**-treated mice during the treatment period (Figure 16C). Furthermore, remarkable tumor destruction induced by **20k** was observed by Hematoxylin-eosin (H&E) staining (Figure 16D). As shown by H&E staining, large areas of necrosis (regions with homogenous pink staining) and karyorrhexis were watched after treatment of **20k**, while Taxol show less tumor destruction, indicating the excellent tumoricidal efficacy of **20k**. These results suggested that **20k** had potential antitumor efficacy against the growth of implanted drug-resistant human NSCLC cells in mice.

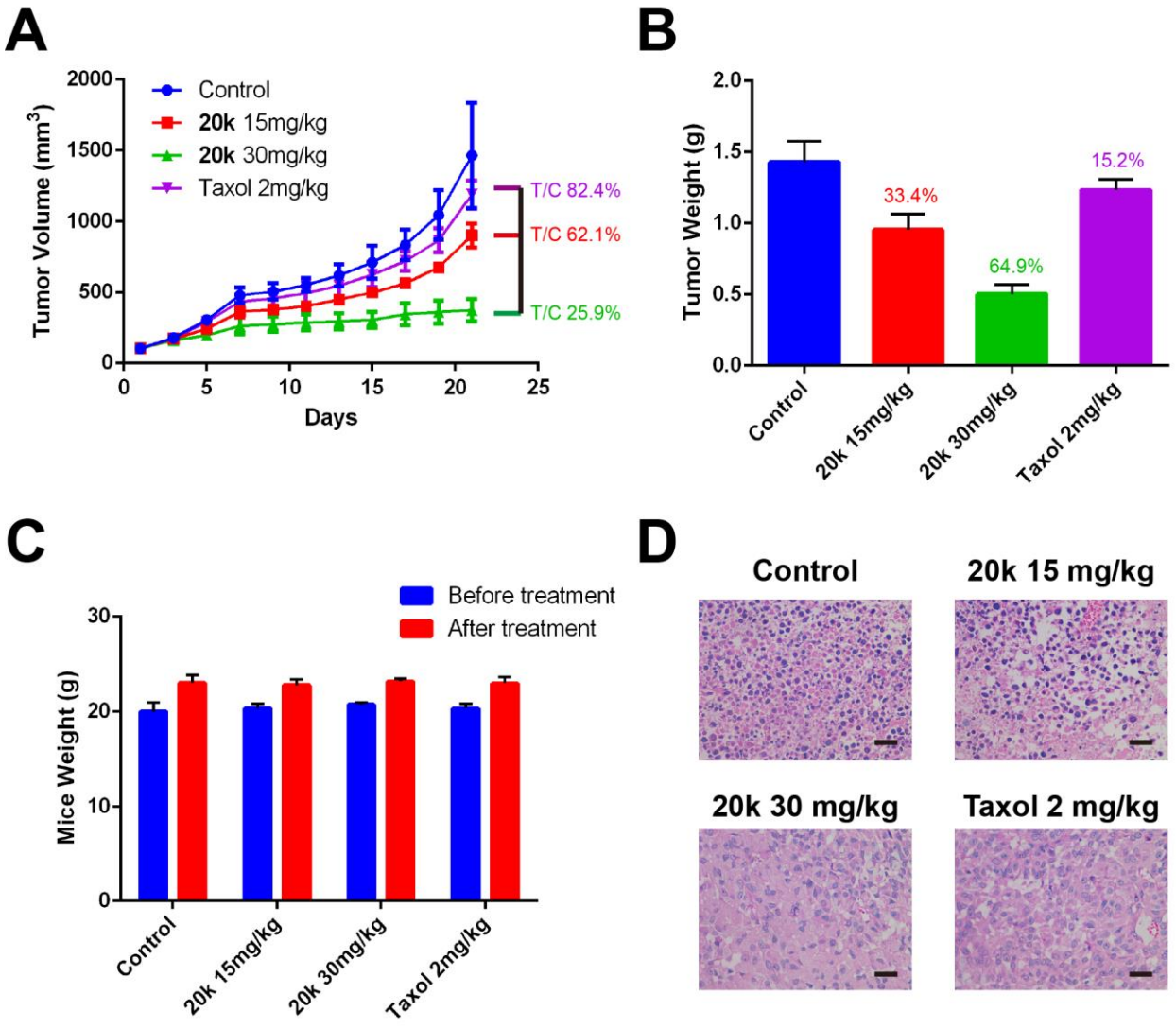

Figure 16. Compound **20k** suppressed the tumor growth in vivo in A549/Taxol tumor xenografts nude model. A549/Taxol tumor-bearing mice were treated with vehicle and **20k** (15 mg/kg and 30 mg/kg). Taxol (2 mg/kg) was selected as the reference. (A) Changes in tumor volume of A549/Taxol tumor-bearing mice after treatment for 3 weeks. (B) Tumor weight after treatment. (C) Mice body weight of the treated mice. (D) H&E stained tissue sections from A549/Taxol tumor-bearing mice after treatment. Scale bars represent 400 μm.

2.7. In Vivo Preliminary Toxicity Studies on Compound 20k. We further examined the acute toxicity of **20k** on the A549/Taxol tumor-bearing nude mice through histopathology and blood biochemistry analysis. After 3 weeks of injection, mice were euthanized, H&E staining of major organs were conducted. The blood was collected for blood biochemistry analysis. As shown in Figure 17A, the heart, liver, spleen, lungs, and kidneys showed no obvious damage after treatment of **20k**, indicating that compound **20k** has no apparent toxicity on mice. Additionally, blood biochemistry test revealed that compound **20k** has less hepatotoxicity, nephrotoxicity and cardiotoxicity in tumor-bearing nude mice, compared to Taxol (Figure 17B), as reflected by the liver function indicators (TP, total protein; ALB, albumin; GLB, globulin, and AST, aspartate aminotransferase), kidney function indicators (BUN, blood urea nitrogen) and myocardial enzyme indicator (LDH, lactate dehydrogenase). These results indicated that compound **20k** had good drug safety with little toxicity to normal tissues and be applied in new cancer therapeutics.

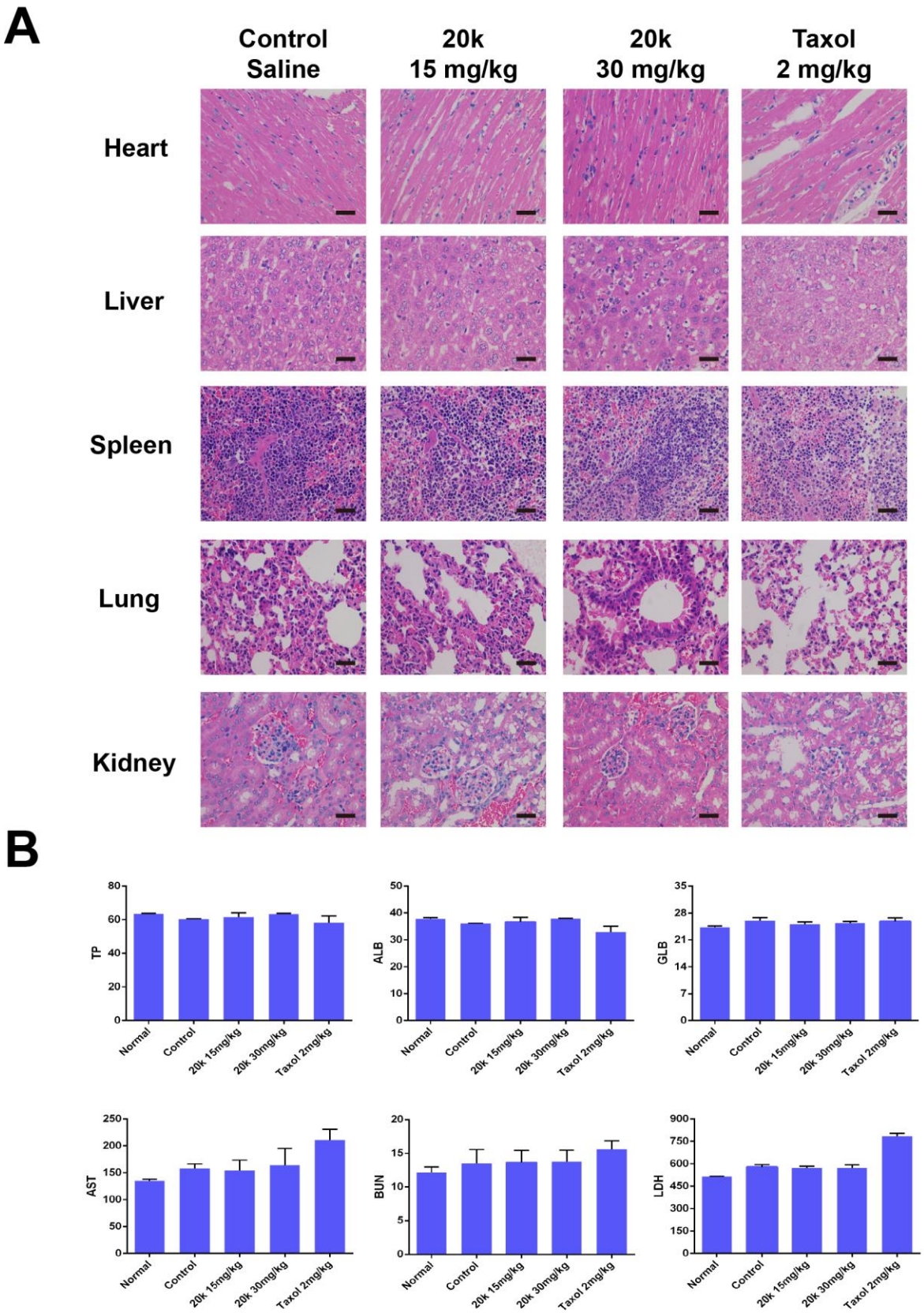
A
Control Saline
20k 15 mg/kg
20k 30 mg/kg
Taxol 2 mg/kg
Heart
Liver
Spleen
Lung
Kidney
B
TP
ALB
GLB
AST
BUN
LDH
Normal
Control
20k 15mg/kg
20k 30mg/kg
Taxol 2mg/kg

Figure 17. Evaluation of **20k**-induced systemic toxicities in vivo. (A) H&E staining of major organs from nude mice after treatment of saline, **20k** (15 mg/kg and 30 mg/kg) and Taxol (2 mg/kg). (B) Blood biochemistry analysis the indicators of TP, ALB, GLB, AST, BUN and LDH in mice. Scale bars represent 400 μm.

2.7. Determination of ROS Generation and GSH Depletion In Vivo. It has been proven that **20k** exerted its antitumor activity by generating ROS through intracellular NQO1 in A549/Taxol cells. We further evaluated the abilities of compound **20k** to induce ROS generation and its effect on the antioxidant system in vivo by examining tumor tissues isolated from A549/Taxol tumor-bearing mice. It is shown that compound **20k** increased the ROS level and reduced the level of GSH (glutathione), which plays a crucial role in maintaining biological redox homeostasis and is an important part of antioxidant system (Figure 18). In conclusion, compound **20k** could induce ROS generation and deplete GSH levels simultaneously so that it can maximally exploit the ROS-mediated cancer cell death.

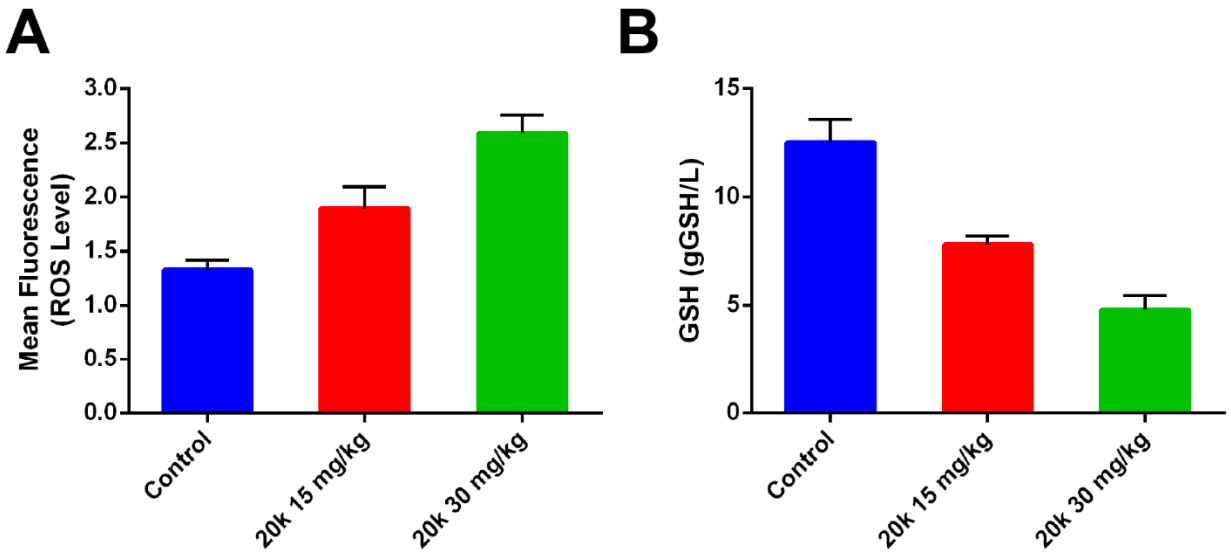

Figure 18. Measurement of ROS and GSH levels in tumor tissues isolated from A549/Taxol tumor-bearing mice. (A) ROS generation. (B) GSH depletion.

3. CONCLUSIONS

In this study, we initially identified that compound **1** was an excellent NQO1 substrate with a tetracyclic non-quinone scaffold through screening of an in-house database. Then compound **1** was selected as a hit compound for further SAR study by a step-by-step modification strategy which led to compound **10** with a simplified indenopyrazinone tricylic scaffold. Concerning both the structure features for NQO1 binding and the electrochemical redox potentials for NQO1 bioreduction, a series of 2,3-dicyano indenopyrazinones were designed, synthesized and biologically evaluated. It was found that the most efficient NQO1 substrate **20k** displayed potent and selective antiproliferative activity against NQO1-overexpressing A549 cells and drug-resistance A549/Taxol cells. Furthermore, pharmacological study demonstrated that **20k** dramatically elevated the intracellular ROS levels through NQO1-catalyzed redox cycling, and induced PARP-1-mediated cell apoptosis in an NQO1- and ROS-dependent manner in A549/Taxol cells. In addition, **20k** significantly suppressed the growth of A549/Taxol xenograft tumors in mice with no apparent toxicity observed in vivo. In conclusion, we discover a new chemotype of non-quinone substrates for NQO1 as effective and selective intracellular ROS generators for developing promising new drugs for the treatment of NQO1-overexpresssing drug-resistant NSCLC.

4. EXPERIMENTAL SECTION

4.1. General Chemistry. All reagents were purchased from commercial sources. Organic solutions were concentrated in a rotary evaporator (BüchiRotavapor) below 55 ℃ under reduced

pressure. Reactions were monitored by thin-layer chromatography (TLC) on 0.25 mm silica gel plates (GF254) and visualized under UV light. Melting points were determined with a Melt-Temp II apparatus. The ^{1}H NMR and ^{13}C NMR spectra were measured on a Bruker AV-300 instrument using deuterated solvents with tetramethylsilane (TMS) as internal standard. EI-MS was collected on shimadzu GCMS-2010 instruments. ESI-mass and high resolution mass spectra (HRMS) were recorded on a Water Q-Tofmicro mass spectrometer. Analytical results are within 0.40% of the theoretical values. The purity (≥95%) of the target compounds is verified by the high performance liquid chromatography (HPLC) study performed on an Agilent C18 (4.6 mm × 150 mm, 3.5 μm) column using a mixture of solvent methanol/water and acetonitrile/water at a flow rate of 0.5mL/min and peak detection at 254 nm under UV.

4.2. Synthesis. General procedure for the synthesis of 2-5. To a solution of 1,2,3-indantrione monohydrate (**21**) (356 mg, 2 mmol) in EtOH (10 mL) was added **22a-c** or **23** (2 mmol) and AcOH (1 mL), the mixture was stirred at room temperature for 2 h. The precipitate was filtered, washed with EtOH, and dried under vacuum to afford the target compounds **2-5** (28%-86%).

11*H*-indeno[1,2-*b*]quinoxalin-11-one (2). Yield: 86%. Yellow solid. mp 225-226 ℃. ^{1}H NMR (300 MHz, $CDCl_3$) δ: 8.24 (d, J = 7.5 Hz, 1H), 8.12 (d, J = 7.5 Hz, 2H), 7.93 (d, J = 6.0 Hz, 1H), 7.85-7.73 (m, 3H), 7.61 (t, J = 7.5 Hz, 1H). ^{13}C NMR (75 MHz, $CDCl_3$) δ: 189.2, 155.9, 148.6, 142.4, 142.0, 140.9, 136.2, 136.0, 131.9, 131.8, 131.0, 129.7, 129.1, 124.1, 121.9. ESI-HRMS m/z $[M+H]^+$ calculated for $C_{15}H_9N_2O$: 233.0709, found: 247.0708. HPLC (90% acetonitrile in water): t_R = 5.989 min, 97.5%.

7,8-Dimethyl-11*H*-indeno[1,2-*b*]quinoxalin-11-one (3). Yield: 82%. Yellow solid. mp 257-258 ℃. ^{1}H NMR (300 MHz, $CDCl_3$) δ: 8.00 (d, J = 6.0 Hz, 1H), 7.90 (s, 1H), 7.86 (d, J = 9.0 Hz,

1H), 7.78 (s, 1H), 7.71 (t, *J* = 7.5 Hz, 1H), 7.54 (t, *J* = 7.5 Hz, 1H), 2.47 (s, 3H), 2.46 (s, 3H). ^{13}C NMR (75 MHz, $CDCl_3$) *δ*: 189.5, 155.4, 147.6, 142.9, 141.3, 141.1, 140.8, 140.2, 135.9, 135.8, 131.4, 130.1, 128.5, 123.9, 121.6, 20.0, 19.7. ESI-HRMS m/z $[M+H]^+$ calculated for $C_{17}H_{13}N_2O$: 261.1022, found: 261.1030. HPLC (70% methanol in water): t_R = 7.532 min, 96.2%. HPLC (90% methanol in water): t_R = 7.015 min, 98.0%.

7,8-Difluoro-11*H*-indeno[1,2-*b*]quinoxalin-11-one (4). Yield: 85%. Yellow solid. mp 255-256 ℃. ^{1}H NMR (300 MHz, $CDCl_3$) *δ*: 8.10 (d, *J* = 9.0 Hz, 1H), 8.03-7.86 (m, 3H), 7.80 (t, *J* = 7.5 Hz, 1H), 7.65 (t, *J* = 7.5 Hz, 1H). ^{13}C NMR (75 MHz, $CDCl_3$) *δ*: 188.7, 156.4, 155.1, 154.9, 153.5, 153.0, 151.6, 151.4, 150.1, 149.9, 148.8, 140.6, 140.3, 140.2, 139.4, 139.2, 136.4, 135.9, 132.4, 124.4, 122.1, 116.9, 116.7, 115.4, 115.1. ESI-HRMS m/z $[M+H]^+$ calculated for $C_{15}H_6F_2N_2NaO$: 291.0340, found: 291.0346. HPLC (90% acetonitrile in water): t_R = 5.149 min, 98.6%.

9*H*-indeno[1,2-*b*]thieno[3,4-*e*]pyrazin-9-one (5). Yield: 73%. Yellow solid. mp 210-212 ℃. ^{1}H NMR (300 MHz, $CDCl_3$) *δ*: 8.24 (d, *J* = 3.0 Hz, 1H), 8.12 (d, *J* = 6.0 Hz, 1H), 7.98-7.95 (m, 2H), 7.81 (t, *J* = 7.5 Hz, 1H), 7.65 (t, *J* = 7.5 Hz, 1H). ESI-HRMS m/z $[M+H]^+$ calculated for $C_{13}H_7N_2OS$: 239.0274, found: 239.0275. HPLC (90% acetonitrile in water): t_R = 6.134 min, 98.5%.

General procedure for the synthesis of 6-7. To a solution of 1,2,3-indantrione monohydrate (**21**) (356 mg, 2 mmol) in EtOH (10 mL) was added **24-25** (2 mmol) and AcOH (0.5 mL), the mixture was stirred at 60 ℃ for 4 h in the air. After cooling to room temperature, the solvent was removed under reduced pressure and residue was purified using silica gel column chromatography (eluent: Petroleum ether/EtOAc 20: 1) to afford the solid **6-7** (28%-30%).

6,7,8,9-Tetrahydro-11*H*-indeno[1,2-*b*]quinoxalin-11-one (6). Yield: 28%. Yellow solid. mp 176-178 ℃. ^{1}H NMR (300 MHz, $CDCl_3$) δ: 7.81 (d, J = 7.5 Hz, 1H), 7.76 (d, J = 7.5 Hz, 1H), 7.62 (t, J = 7.5 Hz, 1H), 7.46 (t, J = 7.5 Hz, 1H), 3.06 (m, J = 3.0 Hz, 4H), 1.97 (m, J = 3.0 Hz, 4H). ^{13}C NMR (75 MHz, $CDCl_3$) δ: 190.5, 157.2, 156.0, 153.0, 144.6, 140.5, 135.3, 133.3, 130.7, 123.9, 120.6, 32.4, 31.6, 21.9, 21.8. ESI-HRMS m/z $[M+H]^+$ calculated for $C_{15}H_{13}N_2O$: 237.1022, found: 237.1026. HPLC (90% acetonitrile in water): t_R = 5.735 min, 98.9%.

9*H*-indeno[1,2-*b*]pyrazin-9-one (7). Yield: 30%. Yellow solid. mp 151-153 ℃. ^{1}H NMR (300 MHz, $CDCl_3$) δ: 8.56 (d, J = 3.0 Hz, 1H), 8.50 (d, J = 3.0 Hz, 1H), 7.90 (d, J = 7.5 Hz, 1H), 7.83 (d, J = 7.5 Hz, 1H), 7.70 (t, J = 7.5 Hz, 1H), 7.54 (t, J = 7.5 Hz, 1H). ^{13}C NMR (75 MHz, $CDCl_3$) δ: 189.8, 160.0, 147.6, 146.1, 144.0, 140.1, 135.8, 133.2, 131.5, 124.2, 121.3. ESI-HRMS m/z $[M+Na]^+$ calculated for $C_{11}H_6N_2NaO$: 205.0372, found: 205.0377. HPLC (90% acetonitrile in water): t_R = 4.677 min, 99.3%.

3-Amino-9*H*-indeno[1,2-*e*][1,2,4]triazin-9-one (8). To a solution of 1,2,3-indantrione monohydrate (**21**) (356 mg, 2 mmol) in EtOH (10 mL) was added Aminoguanidinium nitrate (274 mg, 2 mmoL) and AcOH (1 mL), the mixture was stirred at 70 ℃ for 3 h. The precipitate was filtered, washed with EtOH, and dried under vacuum to afford **8** (262 mg, 66%) as a yellow solid. mp 193-196 ℃. ^{1}H NMR (300 MHz, DMSO) δ: 8.47 (s, 1H), 8.25 (s, 1H), 7.88 (d, J = 7.5 Hz, 1H), 7.83 (d, J = 7.5 Hz, 1H), 7.80-7.75 (m, 2H). ^{13}C NMR (75 MHz, DMSO) δ: 186.6, 164.6, 162.3, 143.8, 137.0, 136.0, 135.7, 134.2, 123.8, 122.8. ESI-HRMS m/z $[M+H]^+$ calculated for $C_{10}H_7N_4O$: 199.0614, found: 199.0618. HPLC (90% acetonitrile in water): t_R = 4.326 min, 98.2%.

9-Oxo-9*H*-indeno[1,2-*b*]pyrazine-2,3-dicarbonitrile (10). To a solution of 1,2,3-indantrione monohydrate (**21**) (356 mg, 2 mmol) in EtOH (10 mL) was added 2,3-diaminomaleonitrile (216

mg, 2 mmol) and AcOH (1 mL), the mixture was stirred at room temperature for 2 h. The precipitate was filtered, washed with EtOH, and dried under vacuum to afford **10** (381 mg, 82%) as a yellow solid. mp 268-269 ℃. ^{1}H NMR (300 MHz, DMSO) δ: 8.11 (d, J = 7.5 Hz, 1H), 7.98-7.90 (m, 2H), 7.82 (t, J = 7.5 Hz, 1H). ^{13}C NMR (75 MHz, DMSO) δ: 186.5, 160.8, 150.8, 138.6, 137.8, 136.3, 135.3, 134.6, 132.5, 125.5, 124.1, 114.8, 114.6. ESI-HRMS m/z $[M+Na]^+$ calculated for $C_{13}H_4N_4NaO$: 255.0277, found: 255.0273. HPLC (90% methanol in water): t_R = 7.532 min, 96.2%.

9*H*-indeno[1,2-*b*]pyrazine-2,3-dicarbonitrile (11). To a suspension of 1,2-indanone (**20**) (146 mg, 1 mmol) in isopropanol (10 mL) was added 2,3-diaminomaleonitrile (**27**) (108 mg, 1 mmol) and the mixture was stirred at room temperature for 4 h, The precipitate was filtered, washed with EtOH, and dried under vacuum to afford **11** (159 mg, 73%). mp 176-178 ℃. ^{1}H NMR (300 MHz, DMSO) δ: 7.81-7.76 (m, 2H), 7.64 (d, J = 3.0 Hz, 1H), 7.62-7.48 (m, 1H), 3.59 (s, 2H). ^{13}C NMR (75 MHz, DMSO) δ: 158.7, 147.6, 137.8, 136.7, 136.6, 135.9, 135.6, 132.7, 127.9, 127.2, 114.6, 113.7, 31.1. ESI-HRMS m/z $[M+H]^+$ calculated for $C_{13}H_7N_4$: 219.0665, found: 219.0667. HPLC (90% acetonitrile in water): t_R = 3.551 min, 99.0%.

General procedure for the synthesis of 12-15. A solution of corresponding sodium alkoxides (2 mmol) or amines (2-6 mmol) was added to a suspension of **10** (464 mg, 2 mmol) in MeOH (10 mL), and the mixture was stirred at room temperature for 4 h. The precipitate was filtered, washed with EtOH, and dried under vacuum to afford the solid **12-15** (37%-87%).

3-Methoxy-9-oxo-9*H*-indeno[1,2-*b*]pyrazine-2-carbonitrile (12). Yield: 87%. Yellow solid. mp 260-262 ℃. ^{1}H NMR (300 MHz, DMSO) δ: 8.11 (d, J = 9.0 Hz, 1H), 7.85-7.81 (m, 2H), 7.71 (t,

J = 7.5 Hz, 1H), 4.24 (s, 3H). ESI-HRMS m/z $[M+Na]^+$ calculated for $C_{13}H_7N_3NaO_2$: 260.0430, found: 260.0436. HPLC (90% methanol in water): t_R = 7.472 min, 99.0%.

3-Ethoxy-9-oxo-9*H*-indeno[1,2-*b*]pyrazine-2-carbonitrile (13). Yield: 82%. Yellow solid. mp 232-234 ℃. ^{1}H NMR (300 MHz, DMSO) δ: 7.90-7.79 (m, 3H), 7.70 (t, *J* = 7.5 Hz, 1H), 4.70 (q, *J* = 6.0 Hz, 2H), 1.47 (t, *J* = 7.5 Hz, 3H). ^{13}C-NMR (75 MHz, DMSO) δ: 186.9, 163.5, 162.0, 140.0, 138.1, 136.3, 135.1, 133.7, 124.2, 122.5, 116.4, 114.7, 65.2, 14.0. ESI-HRMS m/z $[M+H]^+$ calculated for $C_{14}H_{10}N_3O_2$: 252.0768, found: 252.0766. HPLC (90% methanol in water): t_R = 10.776 min, 99.4%.

3-Amino-9-oxo-9*H*-indeno[1,2-*b*]pyrazine-2-carbonitrile (14). Yield: 37%. Yellow-green solid. mp 287-289 ℃. ^{1}H NMR (300 MHz, DMSO) δ: 8.46 (s, 2H), 7.76-7.72 (m, 3H), 7.68-7.63 (m, 1H). ^{13}C NMR (75 MHz, DMSO) δ: 186.7, 163.0, 158.1, 138.2, 135.9, 135.8, 135.5, 133.1, 123.5, 121.9, 115.9, 110.0. ESI-HRMS m/z $[M+Na]^+$ calculated for $C_{12}H_6N_4NaO$: 245.0434, found: 245.0443. HPLC (90% acetonitrile in water): t_R = 4.686 min, 98.8%.

3-(Dimethylamino)-9-oxo-9*H*-indeno[1,2-*b*]pyrazine-2-carbonitrile (15). Yield: 74%. Yellow solid. mp 267-269 ℃. ^{1}H NMR (300 MHz, DMSO) δ: 7.85 (d, *J* = 6.0 Hz, 1H), 7.80-7.74 (m, 2H), 7.67 (t, *J* = 7.5 Hz, 1H), 3.47 (s, 6H). ESI-HRMS m/z $[M+H]^+$ calculated for $C_{14}H_{11}N_4O$: 251.0927, found: 251.0929. HPLC (90% methanol in water): t_R = 8.381 min, 97.6%.

3-Chloro-9-oxo-9*H*-indeno[1,2-*b*]pyrazine-2-carbonitrile (16). A mixture of *tert*-butyl nitrite (0.54 ml, 5 mmol), $CuCl_2$ (0.20 g, 1.5 mmol) and **14** (222 mg, 1 mmol) in anhydrous MeCN (10 mL) was stirred at 65 ℃ for 4 h. The precipitate was filtered out and filtrate was concentrated under reduced pressure. The residue was further purified using silica gel column chromatography using 5-10% petroleum ether to ethylacetate gradient solvent system to afford **16** (140 mg, 58%)

as a yellow solid. mp 229-231 ℃. ^{1}H NMR (300 MHz, DMSO) δ: 8.03 (d, J = 9.0 Hz, 1H), 7.93-7.86 (m, 2H), 7.78 (t, J = 7.5 Hz, 1H). ^{13}C NMR (75 MHz, DMSO) δ: 186.5, 161.6, 153.3, 146.8, 137.0, 135.5, 135.1, 134.4, 127.0, 124.8, 123.3, 114.7. ESI-HRMS m/z $[M+H]^+$ calculated for $C_{12}H_5ClN_3O$: 242.0116, found: 242.0111. HPLC (90% methanol in water): t_R = 8.424 min, 96.2%.

General procedure for the synthesis of 17-18. To a solution of **16** (242 mg, 1 mmol) in anhydrous MeCN (10 mL) was added corresponding alkynes (1.5 mmol), triethylamine (0.16 mL, 1.1 mmol), $Pd(dppf)_2Cl_2$ (69 mg, 0.1 mmol), CuI (17 mg, 0.1 mmol) under a nitrogen atmosphere. The mixture was stirred at 80 ℃ for 3 h under a nitrogen atmosphere. After cooling to room temperature, the precipitate was filtered out and filtrate was concentrated under reduced pressure. The mixture was further purified using silica gel column chromatography (eluent: Petroleum ether/EtOAc 40: 1) to afford the solid **17-19** (24%-36%).

9-Oxo-3-(prop-1-yn-1-yl)-9*H*-indeno[1,2-*b*]pyrazine-2-carbonitrile (17). Yield: 36%. Yellow solid. mp 226-228 ℃. ^{1}H NMR (300 MHz, $CDCl_3$) δ: 8.01 (d, J = 6.0 Hz, 1H), 7.90 (d, J = 9.0 Hz, 1H), 7.78 (t, J = 7.5 Hz, 1H), 7.66 (t, J = 7.5 Hz, 1H) ,2.33 (s, 3H). ESI-HRMS m/z $[M+H]^+$ calculated for $C_{15}H_8N_3O$: 246.0662, found: 246.0664. HPLC (90% acetonitrile in water): t_R = 4.471 min, 98.9%.

3-(Cyclopropylethynyl)-9-oxo-9*H*-indeno[1,2-*b*]pyrazine-2-carbonitrile (18). Yield: 28%. Yellow solid. mp 231-233 ℃. ^{1}H NMR (300 MHz, $CDCl_3$) δ: 8.00 (d, J = 9.0 Hz, 1H), 7.89 (d, J = 7.5 Hz, 1H), 7.76 (t, J = 7.5 Hz, 1H), 1.70 (m, J = 6.0 Hz, 1H) ,1.16-1.13 (m, 4H). ^{13}C NMR (75 MHz, $CDCl_3$) δ: 186.7, 160.2, 144.8, 144.3, 138.5, 136.3, 134.8, 133.3, 130.8, 124.7, 122.7, 114.5, 110.4, 72.0, 10.0, 0.6. ESI-HRMS m/z $[M+H]^+$ calculated for $C_{17}H_{10}N_3O$: 272.0818, found: 272.0818. HPLC (90% acetonitrile in water): t_R = 4.805 min, 99.1%.

9-Oxo-3-(phenylethynyl)-9*H*-indeno[1,2-*b*]pyrazine-2-carbonitrile (19). Yield: 24%. Yellow solid. mp 235-237 ℃. ^{1}H NMR (300 MHz, $CDCl_3$) δ: 7.96 (d, J = 6.0 Hz, 1H), 7.83 (d, J = 6.0 Hz, 1H), 7.73-7.67 (m, 3H), 7.59 (t, J = 7.5 Hz, 1H), 7.46-7.35 (m, 3H). ^{13}C NMR (75 MHz, $CDCl_3$) δ: 186.6, 160.3, 144.8, 144.5, 138.5, 136.4, 134.9, 133.4, 132.5, 131.1, 130.7, 128.3, 124.7, 122.8, 119.6, 114.5, 102.8, 84.5. ESI-HRMS m/z $[M+H]^+$ calculated for $C_{20}H_{10}N_3O$: 308.0818, found: 308.0820. HPLC (90% acetonitrile in water): t_R = 4.952 min, 96.4%.

General procedure for the synthesis of 20a-m. 2,3-Diaminomaleonitrile (**27**) (324 mg, 3 mmol) was added to a suspension of substituted 1,2-indanone (**29a-m**) (3 mmol) in isopropanol (20 mL). The mixture was stirred at room temperature for 6 h, The precipitate was filtered, washed with EtOH, and dried under vacuum. The crude product was used without further purification. To a suspension of compound **30a-m** (1 mmol) in AcOH (5 mL) was added $K_2Cr_2O_7$ (542 mg, 1.8 mmol), and the mixture was heated to 100 ℃ for 1 h. After cooling to room temperature, the solvent was evaporated under reduced pressure, and the mixture was further purified using silica gel column chromatography to afford the solid **20a-m** (42%-66%).

6-Methyl-9-oxo-9*H*-indeno[1,2-*b*]pyrazine-2,3-dicarbonitrile (20a). Yield: 50%. Yellow solid. mp 231-233 ℃. ^{1}H NMR (300 MHz, DMSO) δ: 7.96 (s, 1H), 7.87 (d, J = 6.0 Hz, 1H), 7.64 (d, J = 9.0 Hz, 1H), 2.53 (s, 3H). ^{13}C NMR (75 MHz, DMSO) δ: 185.6, 160.3, 150.8, 149.1, 138.4, 135.2, 134.0, 133.6, 131.9, 125.1, 124.0, 114.3, 114.1, 21.8. ESI-HRMS m/z $[M+Na]^+$ calculated for $C_{14}H_6N_4NaO$: 269.0434, found: 269.0425. HPLC (90% acetonitrile in water): t_R = 4.277 min, 98.7%.

8-Methoxy-9-oxo-9*H*-indeno[1,2-*b*]pyrazine-2,3-dicarbonitrile (20b). Yield: 42%. Yellow solid. mp 229-231 ℃. ^{1}H NMR (300 MHz, DMSO) δ: 7.90 (t, J = 9.0 Hz, 1H), 7.65-7.59 (m, 1H),

7.48 (d, J = 9.0 Hz, 1H), 4.02 (s, 3H). ESI-HRMS m/z $[M+Na]^+$ calculated for $C_{14}H_6N_4NaO_2$: 285.0383, found: 285.0380. HPLC (90% acetonitrile in water): t_R = 4.341 min, 97.2%.

7-Methoxy-9-oxo-9*H*-indeno[1,2-*b*]pyrazine-2,3-dicarbonitrile (20c). Yield: 50%. Yellow solid. mp 221-223 ℃. ^{1}H-NMR (300 MHz, DMSO) δ: 7.96 (d, J = 6.0 Hz, 1H), 7.62 (s, 1H), 7.32 (d, J = 9.0 Hz, 1H), 4.03 (s, 3H). ^{13}C NMR (75 MHz, DMSO) δ: 184.1, 166.7, 159.7, 151.3, 141.1, 133.9, 132.2, 129.0, 127.6, 120.6, 114.3, 114.1, 108.2, 56.8. ESI-HRMS m/z $[M+Na]^+$ calculated for $C_{14}H_6N_4NaO_2$: 285.0383, found: 285.0385. HPLC (90% acetonitrile in water): t_R = 4.188 min, 99.0%.

6-Methoxy-9-oxo-9*H*-indeno[1,2-*b*]pyrazine-2,3-dicarbonitrile (20d). Yield: 66%. Yellow solid. mp 224-226 ℃. ^{1}H NMR (300 MHz, DMSO) δ: 7.94 (d, J = 6.0 Hz, 1H), 7.62 (s, 1H), 7.31 (d, J = 7.5 Hz, 1H), 4.01 (s, 3H). ^{13}C NMR (75 MHz, DMSO) δ: 184.2, 166.6, 159.7, 151.3, 141.1, 133.9, 132.2, 129.0, 127.6, 120.6, 114.3, 114.0, 108.2, 56.8. ESI-HRMS m/z $[M+Na]^+$ calculated for $C_{14}H_6N_4NaO_2$: 285.0383, found: 285.0383. HPLC (90% acetonitrile in water): t_R = 4.164 min, 96.1%.

6-Hydroxy-9-oxo-9*H*-indeno[1,2-*b*]pyrazine-2,3-dicarbonitrile (20e). Yield: 44%. Orange solid. mp 243-246 ℃. ^{1}H NMR (300 MHz, DMSO) δ: 9.77 (s, 1H), 7.36 (d, J = 9.0 Hz, 1H), 7.09 (dd, J = 9.0 Hz, J = 3.0 Hz, 1H), 6.92 (d, J = 3.0 Hz, 1H). ESI-HRMS m/z $[M+Na]^+$ calculated for $C_{13}H_4N_4NaO_2$: 271.0226, found: 271.0218. HPLC (90% acetonitrile in water): t_R = 3.968 min, 98.0%.

6-Fluoro-9-oxo-9*H*-indeno[1,2-*b*]pyrazine-2,3-dicarbonitrile (20f). Yield: 60%. Yellow solid. mp 220-222 ℃. ^{1}H NMR (300 MHz, DMSO) δ: 8.08-8.04 (m, 2H), 7.69-7.62 (m, 1H). ESI-HRMS

m/z $[M+Na]^+$ calculated for $C_{13}H_3FN_4NaO$: 273.0183, found: 273.0180. HPLC (90% acetonitrile in water): t_R = 4.152 min, 98.9%.

6-Trifluoromethyl-9-oxo-9*H*-indeno[1,2-*b*]pyrazine-2,3-dicarbonitrile (20g). Yield: 47%. Yellow solid. mp 248-250 ℃. ^{1}H NMR (300 MHz, DMSO) δ: 8.22 (s, 1H), 7.98 (d, J = 9.0 Hz, 1H), 7.87 (d, J = 7.5 Hz, 1H). ESI-HRMS m/z $[M+H]^+$ calculated for $C_{14}H_4F_3N_4O$: 301.0332, found: 301.0331. HPLC (90% acetonitrile in water): t_R = 4.343 min, 99.3%.

6,7-Dimethyl-9-oxo-9*H*-indeno[1,2-*b*]pyrazine-2,3-dicarbonitrile (20h). Yield: 60%. Yellow solid. mp 233-235 ℃. ^{1}H NMR (300 MHz, $CDCl_3$) δ: 7.82 (s, 1H), 7.74 (s, 1H), 2.49 (s, 3H), 2.46 (s, 3H). ^{13}C NMR (75 MHz, DMSO) δ: 185.8, 160.6, 150.9, 148.0, 144.8, 136.2, 134.0, 133.9, 131.4, 125.8, 124.3, 114.4, 114.1, 20.3, 20.0. ESI-HRMS m/z $[M+Na]^+$ calculated for $C_{15}H_8N_4NaO$: 283.0590, found: 283.0583. HPLC (90% acetonitrile in water): t_R = 4.403 min, 96.0%.

6,7-Dimethoxy-9-oxo-9*H*-indeno[1,2-*b*]pyrazine-2,3-dicarbonitrile (20i). Yield: 62%. Red solid. mp 278-280 ℃. ^{1}H NMR (300 MHz, DMSO) δ: 7.56 (s, 1H), 7.48 (s, 1H), 4.03 (s, 3H), 3.95 (s, 3H). ESI-HRMS m/z $[M+Na]^+$ calculated for $C_{15}H_8N_4NaO_3$: 315.0489, found: 315.0495. HPLC (90% acetonitrile in water): t_R = 4.482 min, 98.1%.

5,8-Dimethoxy-9-oxo-9*H*-indeno[1,2-*b*]pyrazine-2,3-dicarbonitrile (20j). Yield: 48%. Red solid. mp 270-272 ℃. ^{1}H NMR (300 MHz, DMSO) δ: 7.62 (d, J = 9.0 Hz, 1H), 7.50 (d, J = 9.0 Hz, 1H), 4.00 (s, 3H), 3.97 (s, 3H). ^{13}C NMR (75 MHz, DMSO) δ: 184.6, 160.9, 156.6, 154.0, 151.6, 133.7, 133.4, 130.5, 130.4, 114.4, 114.1, 107.1, 105.6, 56.9, 56.5. ESI-HRMS m/z $[M+H]^+$ calculated for $C_{15}H_9N_4O_3$: 293.0669, found: 293.0676. HPLC (90% acetonitrile in water): t_R = 4.487 min, 98.8%.

6,7-Difluoro-9-oxo-9*H*-indeno[1,2-*b*]pyrazine-2,3-dicarbonitrile (20k). Yield: 55%. Yellow solid. mp 204-206 ℃. ^{1}H NMR (300 MHz, $CDCl_3$) δ: 7.93-7.88 (m, 1H), 7.85-7.80 (m, 1H). ^{13}C NMR (75 MHz, DMSO) δ: 184.2, 159.2, 156.5, 156.4, 155.0, 154.9, 154.4, 154.3, 153.0, 152.9, 150.7, 136.4, 134.6, 133.9, 132.5, 115.8, 115.7, 114.6, 114.4, 114.3, 114.2. ESI-HRMS m/z $[M+Na]^+$ calculated for $C_{13}H_2F_2N_4NaO$: 291.0089, found: 291.0092. HPLC (90% acetonitrile in water): t_R = 4.185 min, 98.8%.

5,8-Difluoro-9-oxo-9*H*-indeno[1,2-*b*]pyrazine-2,3-dicarbonitrile (20l). Yield: 44%. Orange solid. mp 210-212 ℃. ^{1}H NMR (300 MHz, DMSO) δ: 7.59-7.49 (m, 1H), 7.47-7.17 (m, 1H). ESI-HRMS m/z $[M+Na]^+$ calculated for $C_{13}H_2F_2N_4NaO$: 291.0089, found: 291.0086. HPLC (90% acetonitrile in water): t_R = 4.165 min, 98.3%.

6,7-Dichloro-9-oxo-9*H*-indeno[1,2-*b*]pyrazine-2,3-dicarbonitrile (20m). Yield: 48%. Yellow solid. mp 236-238 ℃. ^{1}H NMR (300 MHz, DMSO) δ: 8.48 (s, 1H), 8.30 (s, 1H). ESI-HRMS m/z $[M]^-$ calculated for $C_{13}H_2Cl_2N_4O$: 299.9606, found: 299.9600. HPLC (90% acetonitrile in water): t_R = 4.319 min, 97.6%.

4.3. Molecular Modeling. A docking study was performed using the crystal structure of the human NQO1 complex with ARH019 (PDB code: 1H69 and resolution 1.86 Å). Compounds were imported to Discovery Studio 4.0, and the 3D conformation was generated by the "Prepare Ligands" protocol at pH 7.0. Then, compounds were energy minimized in CHARMm force field for docking. The molecular docking was carried out using GOLD 5.1 software in combination with ChemScore scoring function. The protein was prepared and the active site was defined as being any volume within 8 Å of the original ligand ARH019 in 1H69. The number of genetic algorithm (GA) run was set to 10, then each GOLD run was saved and docking was terminated

when the top ten solutions attained root-mean-square deviation (RMSD) values within 1.5 Å. The best output poses of ligands generated were analyzed based on hydrogen bonds and van der Waals interactions to the enzyme. The best poses were visualized with PyMol.

4.4. Electrochemistry. Cyclic voltammetry (CV) for the selected compounds was conducted using a model CS120 Electrochemical Analyzer (CH Instruments) equipped with a conventional three-electrode system. The system consisted of a glassy carbon (GC) electrode as the working electrode, a Pt wire as the counter electrode and an Ag/AgCl, Cl^- (sat.) as the reference electrode. All electrodes were contained in a one-compartment electrochemical cell with a volumetric capacity of 10 mL. The reference electrode and the salt bridge were calibrated by voltammetry relative to E_{redox} for Ferrocene (0/+) couple in DMF/Bu_4NPF_6, to allow the measured E_{redox} values for the non-quinones to be quoted relative to Ferrocene (0/+). Electrochemical reduction was performed in aprotic media (DMF + Bu_4NPF_6 0.1 M) at room temperature (22-25 ℃). Each compound (1 mM) was added to the supporting electrolyte, and the solution was deoxygenated with nitrogen and kept under a continuous flow of nitrogen during the experiment. All data were recorded at a potential range between 0.00 and -2.00 V and at potential sweep rates of 50 mV/s.

4.5. Pharmacology. In Vitro NQO1 Reduction Assay. All of the synthesized compounds were monitored as NQO1 substrates using an NADPH recycling assay and recombinant NQO1 (DT-diaphorase, EC 1.6.5.5, human recombinant, Sigma), in which NADPH oxidation to $NADP^+$ was monitored by absorbance (A_{340}) on a Varioskan Flash (Thermo, Waltham, MA). Compounds in DMSO stock (2 μL of 10X stock per well) were added a 96-well plate. NADPH (400 μM) and NQO1 (1.4 μg/mL) in 50 mM potassium phosphate buffer (pH = 7.4) were added to each well (198 μL). Once the 96-well plate was filled with the assay solution except the NADPH solution, it

was placed into the incubator at 37 ℃ and left to sit for 3 min before the measurement. The reaction was initiated by the addition of NADPH solution into the wells, and the absorbance change at 340 nm was measured at 2 s intervals for 5 min at room temperature (22-25 ℃). The linear portion of the absorbance vs time graphs (the first 20 s to 1 min) were fitted and the slops were calculated (velocity). Initial velocities were calculated and results expressed as μmol NADPH oxidized/min/μmol protein. In addition, initial velocities were calculated for a variety of concentrations and Michaelis-Menten curves were generated using Graphpad Prism 6.

As for screening of the in-house compound collection, the tested compound at the concentration of 10 μM was coincubated with NQO1 (1.4 μg/mL) and NADPH (400 μM), and NADPH oxidation to $NADP^+$ in 5 min was monitored by absorbance at 340 nm. N (cycles), defined as the equiv of consumed NADPH divided by the equiv of tested compound, was calculated.

Cell Culture. The multidrug resistant human lung cancer A549/Taxol, A549/VCR (ATCC), human lung cancer A549 (ATCC), human breast cancer MCF-7 (ATCC), and human pancreatic cancer MIA PaCa-2 (ATCC) cell lines were cultured in a humidified, 5% CO_2 atmosphere at 37 ℃ in Roswell Park Memorial Institute medium (RPMI) 1640 (Gibco) or Dulbecco's modified Eagle's medium (DMEM) (Gibco) supplemented with 10% fetal bovine serum (FBS, heated-inactivated, Fisher Scientific) and 1% penicillin/streptomycin. All cell lines were subcultured every 2-3 days.

Cell Viability Assay. Cells were seeded in 96-well plates at a density of 1 x 10^4 cells/mL and allowed to attach overnight. Each compound was added to the wells at concentrations ranging from 1 to 100 μM for 4 h, Plates were then removed and replaced with fresh medium. Plates were incubated at 37 ℃ in a 5% CO_2 atmosphere for 72 h. MTT (3-(4,5-dimethylthiazol-2-yl)-2,5-

diphenyltetrazolium bromide) solution (5 mg/mL) was added and the cells were incubated for another 4 h. The solutions were removed carefully by extraction, the formazan was dissolved in 150 μL of DMSO. The absorbance (OD) was read on a plate at 560 nm. The concentration causing 50% inhibition of cell growth (IC_{50}) was determined. All toxicity experiments were repeated on at least three technical replicates. The data was analyzed using Graphpad Prism 6.

Superoxide Anion Generation in Cell-Free Assay. The superoxide anion generation was monitored using a spectrophotometric assay and cytochrome c as the terminal electron acceptor, in which the reduction rate of cytochrome c was measured by absorbance (A_{550}) on a Varioskan Flash (Thermo, Waltham, MA). Non-quinone compounds (25 μM), cytochrome c (30 μM), NADPH (200 μM), and recombinant NQO1 (0.1-3.0 1.4 μg/mL) (DT-diaphorase, EC 1.6.5.5, human recombinant, Sigma) were mixed in a final volume of 1 mL of 25 mM Tris-HCl solution (pH = 7.4) containing bovine serum albumin (0.7 mg/mL) and 0.1% Tween 20. The reactions were initiated by the addition of NADPH solution into the wells, and the absorbance change at 550 nm was measured at 2 s intervals for 5 min at room temperature (22-25 ℃). Reduction rates were calculated from the liner part of the absorbance vs time graphs (the first 0 to 30 s), and results were expressed as μmol cytochrome c reduced/min/mg protein by using a molar extinction coefficient of 21.1 $mM^{-1}cm^{-1}$ for cytochrome c. The data was analyzed using Graphpad Prism 6.

Measurement of Intracellular ROS Levels. The fluorescent imaging of ROS production was performed on A549/Taxol cells. Cells were seeded at 1×10^6 cells/well in a 6-well plate and were incubated at 37 ℃ under a 5% CO_2 atmosphere for 24 h. Cells were then treated with compounds at the indicated time and dosages, incubated with 10 μM DCFH-DA (Beyotime), DHE (Beyotime), APF (Sigma) for 30 min at 37 ℃, and fixed with 4% formaldehyde for 20 min. The

cells were washed twice with PBS, and fluorescence was observed under a laser scanning confocal microscope (Olympus Fluoview FV1000, Japan).

Western Blot Analysis. Biomarker modulation was determined by Western blot. A549/Taxol cells in Petri dishes were treated with compounds at the indicated ways. The cells were harvested, washed with cold PBS and trypsinized, then the cell lysates were prepared and centrifuged at 12000 rpm for 20 min at 4 ℃. The supernatants were collected and the protein concentration was determined by a bicinchoninic acid (BCA) assay (Thermo, Waltham, MA). Protein samples were separated by SDS-PAGE and then transferred onto PVDF membranes (PerkinElmer, Northwalk, CT, USA). After blocking with 1% bovine serum albumin for 1 h, membranes were incubated at 37 ℃ for 1 h and then at 4 ℃ overnight with primary antibodies. Finally, the membranes were treated with a DyLight 800 labeled secondary antibody at 37 ℃ for 1 h and scanned through the Odyssey infrared imaging System (LO-COR, Lincoln, Nebraska, USA).

Alkaline Comet Assay. DNA damage was assessed by evaluating DNA "comet" tail area and migration distance. A549/Taxol cells were exposed to 10 μM compound **20k** with or without the pretreatment of 50 μM DIC or 10 mM NAC, and incubated for 2 h at 37 ℃. The cell suspensions (3×10^5 cells/mL in PBS) were mixed with 1% low melting temperature agarose at 37 ℃ and transferred onto a CometSlide (KeyGEN). After solidifying for 30 min at 4 ℃, slides were submerged in prechilled lysis buffer (2.5 M NaCl, 100 mM EDTA pH 10, 10 mM Tris Base, 1% sodium lauryl sarcosinate, and 1% Triton X-100) at 4 ℃ for 1 h, then the slides were incubated in alkaline unwinding solution (300 mM NaOH, and 1 mM EDTA) for 30 min at room temperature and washed twice in 1 ×TBE (89.2 mM Tris Base, 89 mM boric acid, and 2.5 mM EDTA disodium salt). Damaged and undamaged DNA was then separated by electrophoresis in 1 ×TBE for 20 min

at 1 V/cm, fixed in 70% ethanol, and stained using propidium iodide (KeyGEN). Comets were visualized using a laser scanning confocal microscope (Olympus IX51, Japan), and images were analyzed by using ImageJ software.

Determination of NAD^+ and ATP Levels. Intracellular NAD^+ levels were measured by a previous assay.[47] In brief, the A549/Taxol cells were seeded at 1×10^6 cells/well in a 6-well plate and allowed to attach overnight. Cells were exposed to 10 μM compound **20k** with or without the pretreatment of 50 μM DIC or 25 mM 3-AB, and harvested at the indicated time. Cell extracts were prepared in 0.5 M perchloric acid, neutralized (1 M KOH, 0.33 M KH_2PO_4/K_2HPO_4, pH 7.5), and centrifuged to remove $KClO_4$ precipitates. Supernatants or NAD^+ standards were incubated for 20 min at 37 ℃ with NAD^+ reaction mixture as described. The absorbance of the extracts was measured at 570 nm and the results were analyzed using Graphpad Prism 6.

Intercellular ATP levels were analyzed using the ATP Assay Kit (Beyotime, China). Briefly, the A549/Taxol cells were seeded at 1×10^6 cells/well in a 6-well plate and allowed to attach overnight. Cells were exposed to 10 μM compound **20k** with or without the pretreatment of 50 μM DIC or 25 mM 3-AB, and harvested at the indicated time. The cells were then lysed and centrifuged at 12000 rpm for 10 min to isolate total protein. Next, the supernatant was added to ATP detection solution and luminescence was immediately detected using Thermo LUMINOSKAN ASCENT. And data were analyzed using Graphpad Prism 6.

Apoptosis Analysis. Cell apoptosis was analyzed using the Annexin V-FITC-PI (FACS) assay. The A549/Taxol cells were seeded at 1×10^6 cells/well in a 6-well plate and allowed to attach overnight. Cells were exposed to compound **20k** at indicated concentrations with or without the pretreatment of 50 μM DIC or 10 mM NAC for 24h. Then the cells harvested and centrifuged

at 1000 g for 5 min, washed with PBS and resuspended. The cells were stained with Annexin V (1:300) for 30 minutes, followed by PI (1:400) staining for 5 minutes. Fluorescence intensity was analyzed using a flow cytometer (FACSCalibur, BD Biosciences, USA).

In Vivo Antitumor Activity. Animal experiments were conducted according to protocols approved by Institutional Animal Care and Use Committee of China Pharmaceutical University. Approximately 5×10^6 A549/Taxol cells suspended in PBS (50 μl) was injected into the flanks of athymic nude mice (7-8 weeks). After the tumors grew to 100-150 mm^3, all the mice were randomized into four groups (five mice for each group) and treated with vehicle, Taxol (2 mg/kg) and compound **20k** (15 mg/kg or 30 mg/kg). Compound **20k** was dissolved in 20% HPβCD and normal saline. Taxol®, manufactured by Bristol-Myers Squibb, was diluted to the appropriate concentration with normal saline. All agents were administered every other day for three weeks by tail vein injection, and tumor growth was monitored and measured every day. After three weeks, mice were euthanized and the average tumor weights were calculated.

Pathology Analysis. A549/Taxol xenograft tumor mice were treated with saline, **20k** (15 mg/kg and 30 mg/kg) and Taxol (2 mg/kg) through tail intravenous injection every other day for three weeks. Nude mice were executed and dissected surgically for evaluation of possible pathological changes. Heart, liver, spleen, lungs, kidneys, and tumors were fixed in 10% buffered formalin, dehydrated in ethanol, embedded in paraffin, and then stained with hematoxylin and eosin (H&E). The pathological changes were captured with a Nikon 80i optical microscope.

Blood Biochemistry Analysis. After treatment with saline, **20k** (15 mg/kg and 30 mg/kg) and Taxol (2 mg/kg), the blood from A549/Taxol xenograft tumor mice was collected and subjected to blood biochemistry test. Blood samples from normal healthy mice were also needed

as a contrast. The blood samples were centrifuged and diluted with acidified isopropanol (containing 0.75 M HCl solution). The supernatant was subjected to blood biochemistry test after being centrifuged. Functional indicators including total protein (TP), albumin (ALB), globulin (GLB), aspartate aminotransferase (AST), blood urea nitrogen (BUN) and lactate dehydrogenase (LDH) were determined.

Determination of ROS and GSH In Vivo. The ROS levels were measured by using DCFH-DA probe mentioned above. The tumor tissues were weighed and put into homogenizer to grind into homogenates, then homogenates were washed with PBS and centrifugation at low speed, the cell suspension was prepared and incubated with 10 μM DCFH-DA for 30 min at 37 ℃, washed twice with PBS and analyzed using a flow cytometer (FACSCalibur, BD Biosciences, USA). The GSH levels were measured using a GSH and GSSG Assay Kit (Beyotime). Briefly, tumor tissues (10 mg) were homogenized in protein removal reagent M solution (100 μL), then being centrifuged at 1000g for 10 min at 4 ℃. The supernatant was measured for total GSH levels using a Varioskan Flash (Thermo, Waltham, MA).

ASSOCIATED CONTENT

Supporting Information.

The Supporting Information is available free of charge on the ACS Publication website at DOI:10.1021/acs.jmedchem.xxxxxxx.

Determination of the NQO1 activity in corresponding cancer cells, and normal hepatic L02 cells, cyclic voltammograms of the representive compounds, β-lap, and the control Ferrocene, doking poses for the representive compounds, possible reduction process for

quinone substrate β-lap by NQO1, HPLC spectra for compound recovery after NQO1 assay, ^{1}H NMR and HRMS spectra for all of the target compounds, and ^{13}C NMR spectra for representative target compounds, HPLC assessment of purity for target compounds (PDF)

Molecular formula strings (CSV)

AUTHOR INFORMATION

Corresponding Author

*(Q. You) Phone & Fax: +86-25-83271351. E-mail: youqd@163.com

*(X. Zhang) Mobile: +86-13913007140. E-mail: zxj@cpu.edu.cn

ORCID

Qidong You: 0000-0002-8587-0122

Xiaojin Zhang: 0000-0002-1898-3071

Notes

The authors declare no competing financial interest.

ACKNOWLEDGMENT

This work was supported by grants from the National Natural Science Foundation of China (No. 81773571, 81603025), Jiangsu Province Funds for Excellent Young Scientists (BK20170088), the Fundamental Research Funds for the Central Universities (2632017ZD03) and the Jiangsu Qing Lan Project and 333 Project. Part of the work was supported by the National Major Science and Technology Project of China (No. 2015ZX09101032, 2017ZX09302003).

ABBREVIATIONS

NQO1, NAD(P)H:quinone oxidoreductase-1; ROS, reactive oxygen species; β-lap, β-lapachone; SAR, structure-activity relationship; HPLC, high performance liquid chromatography; CV, cyclic voltammogram; PDB, protein data bank; equiv, equivalent; MTT, 3-(4,5-dimethylthiazol-2-yl)-2,5-diphenyltetrazolium bromide; NSCLC, non-small cell lung cancer; DCFH-DA, 2′,7′-dichlorodihydrofluorescein diacetate; DHE, dihydroethidium; APF, 3′-(p-aminophenyl) fluorescein; PAR, poly(ADP-ribose) modified protein; PARP-1, poly(ADP-ribose)polymerase-1; DIC, dicoumarol; NAC, N-acetylcysteine; 3-AB, 3-aminobenzamide.

REFERENCES

(1) Oser, M. G.; Niederst, M. J.; Sequist, L. V.; Engelman, J. A. Transformation from non-small-cell lung cancer to small-cell lung cancer: molecular drivers and cells of origin. *Lancet Oncol.* **2015**, 16 (4), 165-172.

(2) Cai, J.; Wu, J.; Zhang, H.; Fang, L.; Huang, Y.; Yang, Y.; Zhu, X.; Li, R.; Li, M. miR-186 downregulation correlates with poor survival in lung adenocarcinoma, where it interferes with cell-cycle regulation. *Cancer Res.* **2013**, 73 (2), 756-766.

(3) Hardin, C.; Shum, E.; Singh, A. P.; Perez-Soler, R.; Cheng, H. Emerging treatment using tubulin inhibitors in advanced non-small cell lung cancer. *Expert Opin. Pharmacother.* **2017**, 18 (7), 701-716.

(4) Gridelli, C.; Peters, S.; Sgambato, A.; Casaluce, F.; Adjei, A. A.; Ciardiello, F. ALK inhibitors in the treatment of advanced NSCLC. *Cancer Treat. Rev.* **2014**, 40 (2), 300-306.

(5) Forde, P. M.; Ettinger, D. S. Targeted therapy for non-small-cell lung cancer: past, present and future. *Expert Rev. Anticancer Ther.* **2013**, 13 (6), 745−758.

(6) Lim, S. H.; Sun, J. M.; Lee, S. H.; Ahn, J. S.; Park, K.; Ahn, M. J. Pembrolizumab for the treatment of non-small cell lung cancer. *Expert Opin. Biol. Ther.* **2016**, 16 (3), 397-406.

(7) Herbst, R. S.; Morgensztern, D.; Boshoff, C. The biology and management of non-small cell lung cancer. *Nature* **2018**, 553 (7689), 446-454.

(8) Frantz, S. Drug approval triggers debate on future direction for cancer treatments. *Nat. Rev. Drug Discov.* **2006**, 5 (2), 91-98.

(9) Melguizo, C.; Prados, J.; Luque, R.; Ortiz, R.; Caba, O.; Alvarez, P. J.; Gonzalez, B.; Aranega, A. Modulation of MDR1 and MRP3 gene expression in lung cancer cells after paclitaxel and carboplatin exposure. *Int. J. Mol. Sci.* **2012**, 13 (12), 16624-16635.

(10) Trachootham, D.; Alexandre, J.; Huang, P. Targeting cancer cells by ROS-mediated mechanisms: a radical therapeutic approach? *Nat. Rev. Drug Discov.* **2009**, 8 (7), 579-591.

(11) Wu, W. S. The signaling mechanism of ROS in tumor progression. *Cancer Metastasis Rev.* **2006**, 25 (4), 695-705.

(12) Li, X.; Fang, P.; Mai, J.; Choi, E. T.; Wang, H.; Yang, X. F. Targeting mitochondrial reactive oxygen species as novel therapy for inflammatory diseases and cancers. *J. Hematol. Oncol.* **2013**, 6, 19.

(13) Gorrini, C.; Harris, I. S.; Mak, T. W. Modulation of oxidative stress as an anticancer strategy. *Nat. Rev. Drug Discov.* **2013**, 12 (12), 931−947.

(14) Schneider, B.; Kulesz-Martin, M. Destructive cycles: the role of genomic instability and adaptation in carcinogenesis. *Carcinogenesis* **2004**, 25 (11), 2033-2044.

(15) Pelicano, H.; Carney, D., Huang, P. ROS stress in cancer cells and therapeutic implications. *Drug Resist. Updates* **2004**, 7 (2), 97−110.

(16) Deavall, D. G.; Martin, E. A.; Horner, J. M.; Roberts, R. Drug-induced oxidative stress and toxicity. *J. Toxicol.* **2012**, 2012, 645460.

(17) Waris, G.; Ahsan, H. Reactive oxygen species: role in the development of cancer and various chronic conditions. *J. Carcinog.* **2006**, 5, 14.

(18) Wang, N.; Wu, Y.; Bian, J.; Qian, X.; Lin, H.; Sun, H.; You, Q.; Zhang, X. Current development of ROS-modulating agents as novel antitumor therapy. *Curr. Cancer Drug Targets* **2017**,17 (2), 122-136.

(19) Raj, L.; Ide, T.; Gurkar, A. U.; Foley, M.; Schenone, M.; Li, X.; Tolliday, N. J.; Golub, T. R.; Carr, S. A.; Shamji, A. F.; Stern, A. M.; Mandinova, A.; Schreiber, S. L.; Lee, S. W. Selective killing of cancer cells by a small molecule targeting the stress response to ROS. *Nature* **2011**, 475 (7355), 231-234.

(20) Zhang, X.; Bian, J.; Li, X.; Wu, X.; Dong, Y.; You, Q. 2-Substituted 3,7,8-trimethylnaphtho[1,2-b]furan-4,5-diones as specific L-shaped NQO1-mediated redox modulators for the treatment of non-small cell lung cancer. *Eur. J. Med. Chem.* **2017**, 138, 616-629.

(21) Ai, Y.; Zhu, B.; Ren, C.; Kang, F.; Li, J.; Huang, Z.; Lai, Y.; Peng, S.; Ding, K.; Tian, J.; Zhang, Y. Discovery of new monocarbonyl ligustrazine-curcumin hybrids for intervention of drug-sensitive and drug-resistant lung cancer. *J. Med. Chem.* **2016**, 59 (5), 1747-1760.

(22) Hall, M. D.; Handley, M. D.; Gottesman, M. M. Is resistance useless? Multidrug resistance and collateral sensitivity. *Trends Pharmacol. Sci.* **2009**, 30 (10), 546-556.

(23) Dharmaraja, A. T. Role of reactive oxygen species (ROS) in therapeutics and drug resistance in cancer and bacteria. *J. Med. Chem.* **2017**, 60 (8), 3221-3240.

(24) Bair, J. S.; Palchaudhuri, R.; Hergenrother, P. J. Chemistry and biology of deoxynyboquinone, a potent inducer of cancer cell death. *J. Am. Chem. Soc.* **2010**, 132 (15), 5469-5478.

(25) Parkinson, E. I.; Bair, J. S.; Cismesia, M., Hergenrother, P. J. Efficient NQO1 substrates are potent and selective anticancer agents. *ACS Chem. Biol.* **2013**, 8 (10), 2173-2183.

(26) Ma, X.; Moore, Z. R.; Huang, G.; Huang, X.; Boothman, D. A.; Gao, J. Nanotechnology-enabled delivery of NQO1 bioactivatable drugs. *J. Drug. Target* **2015**, 23 (7-8), 672-680.

(27) Ma, X.; Huang, X.; Moore, Z.; Huang, G.; Kilgore, J. A.; Wang, Y.; Hammer, S.; Williams, N. S.; Boothman, D. A.; Gao, J. Esterase-activatable β-lapachone prodrug micelles for NQO1-targeted lung cancer therapy. *J. Control. Release* **2015**, 200, 201-211.

(28) Liu, F.; Yu, G.; Wang, G.; Liu, H.; Wu, X.; Wang, Q.; Liu, M.; Liao, K.; Wu, M.; Cheng, X.; Hao, H. An NQO1-initiated and p53-independent apoptotic pathway determines the anti-tumor effect of tanshinone IIA against non-small cell lung cancer. *PloS One* **2012**, 7 (7), e42138.

(29) Bian, J.; Xu, L.; Deng, B.; Qian, X.; Fan, J.; Yang, X.; Liu, F.; Xu, X.; Guo, X.; Li, X.; Sun, H.; You, Q.; Zhang, X. Synthesis and evaluation of (±)-dunnione and its ortho-quinone analogues as substrates for NAD(P)H:quinone oxidoreductase 1 (NQO1). *Bioorg. Med. Chem. Lett.* **2015**, 25 (6), 1244-1248.

(30) Sung, Y. M.; Gayam, S. R.; Hsieh, P. Y.; Hsu, H. Y.; Diau, E. W.; Wu, S. P. Quinone-modified Mn-doped ZnS quantum dots for room-temperature phosphorescence sensing of human cancer cells that overexpress NQO1. *ACS Appl. Mater. Interfaces* **2015**, 7 (46), 25961-25969.

(31) Bey, E. A.; Bentle, M. S.; Reinicke, K. E.; Dong, Y.; Yang, C. R.; Girard, L.; Minna, J. D.; Bornmann, W. G.; Gao, J.; Boothman, D. A. An NQO1- and PARP-1-mediated cell death pathway induced in non-small-cell lung cancer cells by β-lapachone. *Proc. Natl. Acad. Sci. USA* **2007**, 104 (28), 11832-11837.

(32) Parkinson, E. I.; Hergenrother, P. J. Deoxynyboquinones as NQO1-activated cancer therapeutics. *Acc. Chem. Res.* **2015**, 48 (10), 2715-2723.

(33) Hassani, M.; Cai, W.; Holley, D. C.; Lineswala, J. P.; Maharjan, B. R.; Ebrahimian, G. R.; Seradj, H.; Stocksdale, M. G.; Mohammadi, F.; Marvin, C. C.; Gerdes, J. M.; Beall, H. D.; Behforouz, M. Novel lavendamycin analogues as antitumor agents: synthesis, in vitro cytotoxicity, structure-metabolism, and computational molecular modeling studies with NAD(P)H:quinone oxidoreductase 1. *J. Med. Chem.* **2005**, 48 (24), 7733-7749.

(34) Hassani, M.; Cai, W.; Koelsch, K. H.; Holley, D. C.; Rose, A. S.; Olang, F.; Lineswala, W. G.; Gerdes, J. M.; Behforouz, M.; Beall, H. D. Lavendamycin antitumor agents: structure-based design, synthesis, and NAD(P)H:quinone oxidoreductase 1 (NQO1) model validation with molecular docking and biological studies. *J. Med. Chem.* **2008**, 51 (11), 3104-3115.

(35) Newsome, J. J.; Colucci, M. A.; Hassani, M.; Beall, H. D.; Moody, C. J. Benzimidazole- and benzothiazole-quinones: excellent substrates for NAD(P)H:quinone oxidoreductase 1. *Org. Biomol. Chem.* **2007**, 5, 3665-3673.

(36) Baell, J. B.; Holloway, G. A. New substructure filters for removal of pan assay interference compounds (PAINS) from screening libraries and for their exclusion in bioassays. *J. Med. Chem.* **2010**, 53 (7), 2719-2740.

(37) Kuang, Y.; Sechi, M.; Nurra, S.; Ljungman, M.; Neamati, N. Design and synthesis of novel reactive oxygen species inducers for the treatment of pancreatic ductal adenocarcinoma. *J. Med. Chem.* **2018**, 61 (4), 1576-1594.

(38) Li, X.; Bian, J.; Wang, N.; Qian, X.; Gu, J.; Mu, T.; Fan, J.; Yang, X.; Li, S.; Yang, T.; Sun, H.; You, Q.; Zhang, X. Novel naphtha[2,1-d]oxazole-4,5-diones as NQO1 substrates with improved aqueous solubility: design, synthesis, and in vivo antitumor evaluation. *Bioorg. Med. Chem.* **2016**, 24 (5), 1006-1013.

(39) Fryatt, T.; Pettersson, H. I.; Gardipee, W. T.; Bray, K. C.; Green, S. J.; Slawin, A. M.; Beall, H. D.; Moody, C. J. Novel quinolinequinone antitumor agents: structure-metabolism studies with NAD(P)H:quinone oxidoreductase 1 (NQO1). *Bioorg. Med. Chem.* **2004**, 12 (7), 1667-1687.

(40) da Cruz, E. H. G.; Hussene, C. M. B.; Dias, G. G.; Diogo, E. B. T.; de Melo, I. M. M.; Rodrigus, B. L.; da Silva, M. G.; Valenca, W. O.; Camara, C. A.; de Oliveira, R. N.; de Paiva, Y. G.; Goulart, M. O. F.; Cavalcanti, B. C.; Pessoa, C.; da Silva Junior, E. N. 1,2,3-Triazole-, arylamino- and thio-substituted 1,4-naphthoquinones: potent antitumor activity, electrochemical aspects, and bioisosteric replacement of C-ring-modified lapachones. *Bioorg. Med. Chem.* **2014**, 22 (5), 1608-1619.

(41) Bian, J.; Li, X.; Wang, N.; Wu, X.; You, Q.; Zhang, X. Discovery of quinone-directed antitumor agents selectively bioactivated by NQO1 over CPR with improved safety profile. *Eur. J. Med. Chem.* **2017**, 129, 27-40.

(42) Hillard, E. A.; de Abreu, F. C.; Ferreira, D. C.; Jaouen, G.; Goulart, M. O.; Amatore, C. Electrochemical parameters and techniques in drug development, with an emphasis on quinones and related compounds. *Chem. Commun.* **2008**, 23, 2612-2628.

(43) Faig, M.; Bianchet, M. A.; Winski, S.; Hargreaves, R.; Moody, C. J.; Hudnott, A. R.; Ross, D.; Amzel, L. M. Structure-based development of anticancer drugs: complexes of NAD(P)H:quinone oxidoreductase 1 with chemotherapeutic quinones. *Structure* **2001**, 9, 659-667.

(44) Bian, J.; Deng, B.; Xu, L.; Xu, X.; Wang, N.; Hu, T.; Yao, Z.; Du, J.; Yang, L.; Lei, Y.; Li, X.; Sun, H.; Zhang, X.; You, Q. 2-Substituted 3-methylnaphtho[1,2-b]furan-4,5-diones as novel L-shaped ortho-quinone substrates for NAD(P)H:quinone oxidoreductase (NQO1). *Eur. J. Med. Chem.* **2014**, 82, 56-67.

(45) Nolan, K. A.; Doncaster, J. R.; Dunstan, M. S.; Scott, K. A.; Frenkel, A. D.; Siegel, D.; Ross, D.; Barnes, J.; Levy, C.; Leys, D.; Whitehead, R. C.; Stratford, I, J.; Bryce, R. A. Synthesis and biological evaluation of coumarin-based inhibitors of NAD(P)H: quinone oxidoreductase-1 (NQO1). *J. Med. Chem.* **2009**, 52 (22), 7142-7156.

(46) Mendoza, M. F.; Hollabaugh, N. M.; Hettiarachchi, S. H.; McCarley, R. L. Human NAD(P)H:quinone oxidoreductase type I (hNQO1) activation of quinone propionic acid trigger groups. *Biochemistry* **2012**, 51 (40), 8014-8026.

(47) Zhao, H.; Joseph, J.; Fales, H. M.; Sokoloski, E. A.; Levine, R. L.; Vasquez-Vivar, J.; Kalyanaraman, B. Detection and characterization of the product of hydroethidine and intracellular superoxide by HPLC and limitations of fluorescence. *Proc. Natl. Acad. Sci. USA* **2005**, 102 (16), 5727-5732.

(48) Dharmaraja, A. T.; Chakrapani, H. A small molecule for controlled generation of reactive oxygen species (ROS). *Org. Lett.* **2014**, 16 (2), 398-401.

(49) Bentle, M. S.; Reinicke, K. E.; Bey, E. A.; Spitz, D. R.; Boothman, D. A. Calcium-dependent modulation of poly(ADP-ribose) polymerase-1 alters cellular metabolism and DNA repair. *J. Biol. Chem.* **2006**, 281 (44), 33684-33696.

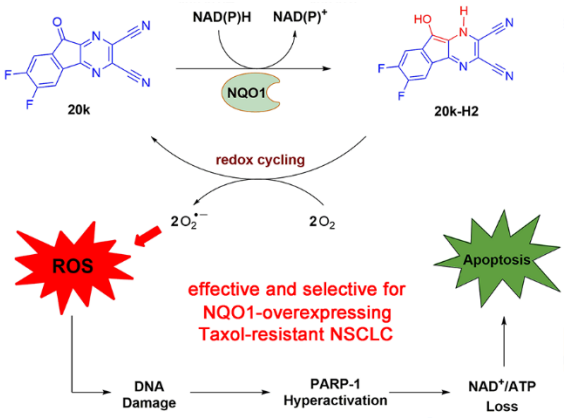

Table of Contents Graphic

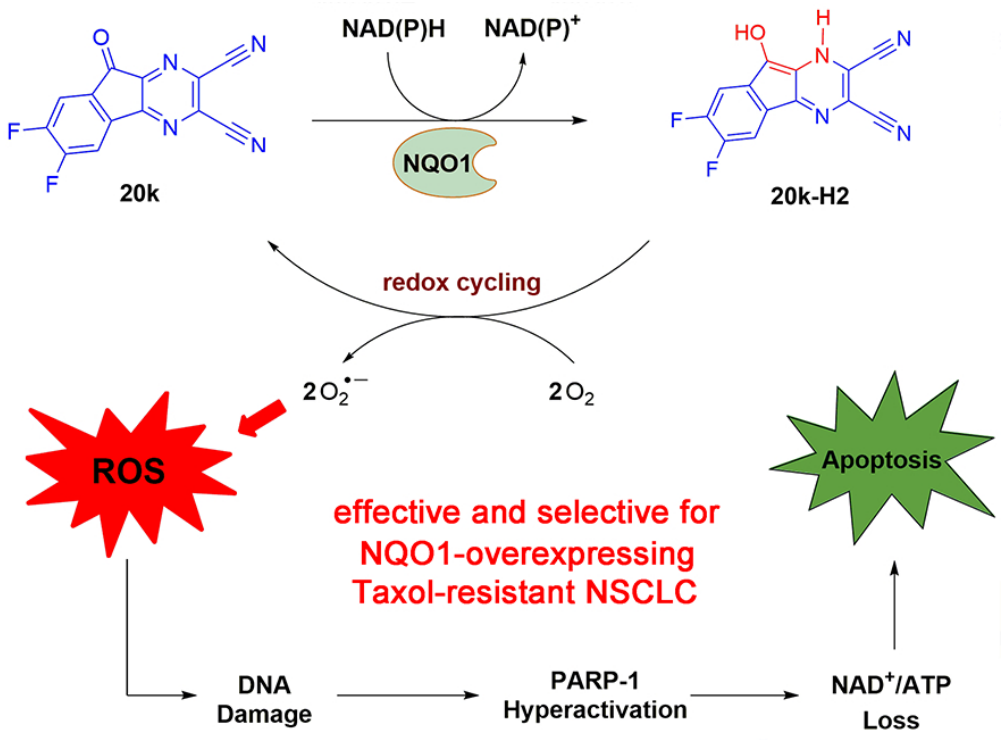

74x55mm (300 x 300 DPI)